communications biology

Article

https://doi.org/10.1038/s42003-024-06762-w

TIM-3 on myeloid cells promotes pulmonary inflammation through increased production of galectin-3

Ki Sun Kim [1], Chanju Lee [1,2], Hyung-Seok Kim [1], Su Jeong Gu [1], Hee Jung Yoon [2], Su Bin Won [1,2], Ho Lee [1], Yong Sun Lee [1], Sang Soo Kim [3], Lawrence P. Kane [4] & Eun Jung Park [1,2] ✉

T cell immunoglobulin and mucin-containing molecule 3 (TIM-3) exhibits unique, cell type- and context-dependent characteristics and functions. Here, we report that TIM-3 on myeloid cells plays essential roles in modulating lung inflammation. We found that myeloid cell-specific TIM-3 knock-in (FSF-TIM3/*LysM*-Cre^{+}) mice have lower body weight and shorter lifespan than WT mice. Intriguingly, the lungs of FSF-TIM3/*LysM*-Cre^{+} mice display excessive inflammation and features of disease-associated pathology. We further revealed that galectin-3 levels are notably elevated in TIM-3-overexpressing lung-derived myeloid cells. Furthermore, both TIM-3 blockade and GB1107, a galectin-3 inhibitor, ameliorated lung inflammation in FSF-TIM3/*LysM*-Cre$^{+/-}$ mice. Using an LPS-induced lung inflammation model with myeloid cell-specific TIM-3 knock-out mice, we demonstrated the association of TIM-3 with both lung inflammation and galectin-3. Collectively, our findings suggest that myeloid TIM-3 is an important regulator in the lungs and that modulation of TIM-3 and galectin-3 could offer therapeutic benefits for inflammation-associated lung diseases.

T cell immunoglobulin and mucin-containing molecule 3 (TIM-3) is an immune checkpoint molecule that consists of an immunoglobulin variable domain, a mucin domain, a transmembrane domain, and a cytoplasmic tail. It was originally identified as a Th1-specific cell surface protein that regulates the severity of experimental autoimmune encephalomyelitis (EAE)[1]. However, subsequent studies have shown that it is also expressed on other types of T cells and non-T cells, including macrophages (MΦ), dendritic cells (DCs), natural killer (NK) cells, and monocytes[2–4]. TIM-3 has been increasingly suggested to exert diverse immunomodulatory functions and thereby affect the pathogenesis of multiple diseases, including autoimmune diseases, viral infections, ischemia, and tumors[1,5–7]. Recently, as increasing attention has focused on the development of immune checkpoint blockade therapies against multiple of diseases, TIM-3 has emerged as a next-generation therapeutic target for immunotherapy[8,9]. Unlike the first-generation immune checkpoint molecules such as PD-1 and CTLA4, TIM-3 exhibits unique context-dependent characteristics and exerts specific roles, depending on the cell types and activation or differentiation status[10,11]. However, little is known about the clinically relevant regulation and functions of TIM-3 in a given situation or the detailed underlying mechanisms that function in specific cells and conditions.

The lungs are continuously exposed to allergens, environmental and endogenous insults, and pathological microbes. Innate immune cells, which are at the forefront of immune responses in the lungs, function as sentinel immune cells or guardians that regulate both the primary initiation and resolution of inflammation in the lungs[12]. Resident and infiltrating myeloid cells, such as macrophage populations within the lungs, are finely regulated to maintain a balance between exerting strong immunity and preventing excessive inflammation. Myeloid cells represent the most abundant immune cells of the lungs; during the course of inflammation, they coordinate the immune regulation, such as by producing a range of inflammatory mediators and engaging in crosstalk with other immune cells and structural cells in the lungs[13,14]. Persistent activations of myeloid cells and abnormal myeloid cell-driven inflammations can lead to unresolved lung injury and impaired gas exchange. These are common features of acute and chronic lung diseases such as acute lung injury (ALI), acute respiratory distress syndrome (ARDS), chronic obstructive pulmonary disease (COPD), allergic asthma, lung cancer and idiopathic pulmonary fibrosis

[1]Department of Cancer Biomedical Science, Graduate School of Cancer Science and Policy, National Cancer Center, Goyang-si, Gyeonggi-do, 10408, Republic of Korea. [2]Immuno-oncology Branch, National Cancer Center, Goyang-si, Gyeonggi-do, 10408, Republic of Korea. [3]Radiological Science Branch, National Cancer Center, Goyang-si, Gyeonggi-do, 10408, Republic of Korea. [4]Department of Immunology, University of Pittsburgh, Pittsburgh, PA, 15213, USA.
✉e-mail: ejpark@ncc.re.kr

(IPF)[15]. Thus, increasing attention has focused on the therapeutic modulation of abnormally inflamed myeloid cells in lung diseases[16,17].

Galectin-3 is the only chimera-type member of the β-galactoside-binding lectin family and has a C-terminal carbohydrate recognition domain (CRD) and tyrosine-rich N-terminal domain. Galectin-3 has been found in the nucleus and cytoplasm, at the cell surface, and in the extracellular milieu of several cell types[18,19]. Inside and outside of cells, galectin-3 has multiple functions in modulating immune and inflammatory responses, for example, by interacting with various molecules under physiological and pathophysiological conditions[20,21]. Clinical and experimental studies have implicated galectin-3 in the development of diverse inflammation-associated disease types, including cardiovascular disease, autoimmune disease, and viral infection[22–24]. Galectin-3 is elevated in the lungs of patients with COPD, IPF, asthma, and viral-induced ARDS[25–27]. Galectin-3 can bind several cell surface glycoproteins via its CRD domain and oligomerize via its N-terminus or CRD. Intracellular and extracellular galectin-3 interact with multiple inflammation-associated molecules, including bcl-2, TLR4, TREM2, CD147, and CD98[28–32]. The interactions and crosstalk of galectin-3 with various intra- and extracellular proteins are closely linked to cellular functions and inflammation-associated diseases[33].

We have been investigating the context-dependent characteristics of TIM-3, especially in innate immune cells under pathophysiological conditions. Our previous findings suggest that TIM-3 plays specific intra- and intercellular immunoregulatory roles in myeloid cells, and that, under certain conditions, these functions are distinct from those exerted by TIM-3 expressed on T cells[6,7]. To further explore the distinctive characteristics of TIM-3 in myeloid cells, we established conditional myeloid cell-specific TIM-3 knock-in and knock-out mice. Using these mice, we herein obtained interesting findings that myeloid cell-expressed TIM-3 significantly impacts lung pathophysiology. Specifically, TIM-3 knock-in mice exhibit distinct features and abnormalities in the lungs and that galectin-3 is closely associated with TIM-3-mediated inflammatory responses. These results suggest that TIM-3 on myeloid cells may modulate the disease-associated inflammatory responses of the lungs, indicating potential therapeutic strategies for inflammation-associated lung diseases.

Results

Myeloid cell-specific TIM-3 knock-in mice have a characteristic gross appearance and short lifespan

To assess the distinctive characteristics of TIM-3 in myeloid cells, we generated a TIM-3 conditional knock-in mouse model (FSF-TIM3/*LysM*-Cre) in which TIM-3 expression is driven in a *LysM*-Cre-dependent manner (Fig. 1a and Supplementary Fig. 1a)[34,35]. Flox-stop-flox TIM-3 (FSF-TIM3) mice were bred with *LysM*-Cre mice to overexpress TIM-3 on myeloid cells (FSF-TIM3/*LysM*-Cre$^{+/+}$) (Fig. 1a and Supplementary Fig. 1b). Interestingly, FSF-TIM3/*LysM*-Cre$^{+/+}$ mice and FSF-TIM3/*LysM*-Cre$^{+/-}$ were both characterized by a lower body weight and smaller size than FSF-TIM3 WT mice (Fig. 1a). To further examine these findings, we measured their body weights and monitored survivals for the indicated periods. FSF-TIM3/*LysM*-Cre$^{+/+}$ and FSF-TIM3/*LysM*-Cre$^{+/-}$ mice consistently weighed less than WT mice, with these differences increasing with age from 4 to 20 weeks (Fig. 1b). Additionally, the survival rate and mean lifespan of FSF-TIM3/*LysM*-Cre$^{+/+}$ and FSF-TIM3/*LysM*-Cre$^{+/-}$ mice were significantly reduced compared with WT mice (Fig. 1c).

We thus asked how TIM-3 overexpression in myeloid cells affects the gross appearance and survival rates of mice. First, we examined the feeding behavior of FSF-TIM3/*LysM*-Cre$^{+/-}$ mice compared to WT mice. As shown in Supplementary Fig. 2a, FSF-TIM3/*LysM*-Cre$^{+/-}$ mice consumed very slightly less food than WT mice at the early age of 4 to 8 weeks. Considering the difference in body weight, there was no significant difference in food intake behavior between FSF-TIM3/*LysM*-Cre$^{+/-}$ mice and WT mice during this period. However, the food intake of FSF-TIM3/*LysM*-Cre$^{+/-}$ mice began to significantly differ from that of WT mice at approximately 15 weeks of age, coinciding with a notable variation in body weights. In addition, insulin and ALT levels did not significantly differ between FSF-TIM3/*LysM*-Cre$^{+/-}$ mice and WT mice at an early age, between 4 and 7 weeks (Supplementary Fig. 2b–d).

Next, we performed diagnostic whole-body imaging to examine internal organs and tissues using [^{18}F]-2-fluoro-2-deoxy-D-glucose ([^{18}F]FDG) and positron emission tomography (PET) with computed tomography (CT). Interestingly, FSF-TIM3/*LysM*-Cre$^{+/+}$ mice showed considerably high [^{18}F]FDG uptakes in the areas of lungs, compared with WT mice (Fig. 1d). Elevated FDG uptake was seen on axial and coronal PET/CT images of FSF-TIM3/*LysM*-Cre$^{+/+}$ mice, and the intensity was increased with age from 4 to 14 weeks (Fig. 1e). However, no differences were found in the lung areas of WT mice between the ages of 4 and 14 weeks (Supplementary Fig. 3a). In addition, no significant differences in [^{18}F]FDG uptake were observed in other organs including the brains, of age-matched FSF-TIM3/*LysM*-Cre$^{+/+}$ and WT mice (Supplementary Fig. 3b). Taken together, these findings suggest that TIM-3 overexpression in myeloid cells may influence the pathological (health) conditions, specifically lungs, gross appearance, and survival of FSF-TIM3/*LysM*-Cre$^{+/+}$ and FSF-TIM3/*LysM*-Cre$^{+/-}$ mice.

Mice with conditional TIM-3 overexpression in myeloid cells display histopathological abnormalities with excessive inflammation in the lungs

To confirm the results from PET/CT, we examined the condition of various organs, including the lungs, by performing necropsies on WT and FSF-TIM3/*LysM*-Cre$^{+/-}$ mice of 5-week-old. We then obtained PBS-perfused images of major thoracic organs, including the heart, lungs, and thymus, as well as abdominal organs, including the liver, spleen, and kidney, from WT and FSF-TIM3/*LysM*-Cre$^{+/-}$ mice (Fig. 2a and Supplementary Fig. 4a). Consistent with the results of PET/CT, the condition of the lungs of FSF-TIM3/*LysM*-Cre$^{+/-}$ mice was different from that in WT mice. No other organs were found to be significantly different from those in WT at 5-week-old.

We then carefully examined the lungs of FSF-TIM3/*LysM*-Cre$^{+/-}$ mice at the indicated weeks of age. As shown in Fig. 2b, c, the lungs of FSF-TIM3/*LysM*-Cre$^{+/-}$ mice were enlarged and inflamed compared to those of FSF-TIM3 mice. The differences in size, inflammation, and lung weights between WT and FSF-TIM3/*LysM*-Cre$^{+/-}$ mice significantly increased with age, from 4 to 14 weeks. To investigate the lungs more precisely, we performed histopathological analysis of hematoxylin and eosin (H&E)-stained sections containing all lung lobes. We found that the lungs of FSF-TIM3/*LysM*-Cre$^{+/-}$ mice displayed disease-associated features, such as alteration of microscopic structures including airways, alveoli, air spaces, and alveolar septa. We also observed numerous cell infiltrates in the obvious lung legions of FSF-TIM3/*LysM*-Cre$^{+/-}$ mice (Fig. 2d). Quantitative characterization of the H&E-stained images revealed that the lung legions of FSF-TIM3/*LysM*-Cre$^{+/-}$ mice showed increase in total cell numbers, tissue area, and tissue density, with a decrease of airspace area, compared to control regions from WT mice (Fig. 2e–h).

To evaluate the above results, we generated T cell-specific TIM-3 overexpressing mice using the *Lck*-Cre system and examined whether the conditional overexpression of TIM-3 in T cells also leads to lung abnormalities. As shown in Fig. 3a, we did not observe significant differences in body weights between FSF-TIM3/*Lck*-Cre$^{+/+}$ mice and WT mice up to 20 weeks of age. In addition, there were no significant signs of inflammation in the lungs of FSF-TIM3/*Lck*-Cre$^{+/+}$ mice (Fig. 3b). These results further support that TIM-3 overexpression in myeloid cells is closely associated with lung abnormalities in FSF-TIM3/*LysM*-Cre^{+} mice.

Inflammation-associated immune cells are abundant in the lungs and BALF of FSF-TIM3/*LysM*-Cre$^{+/+}$ mice

The above results raised the question of whether TIM-3 overexpression in myeloid cells could indeed influence inflammatory events in the lungs. To address this possibility, we harvested lung tissues from WT and FSF-TIM3/*LysM*-Cre$^{+/+}$ mice and used RT-PCR to determine the levels of representative inflammation-associated cytokines. Consistent with our

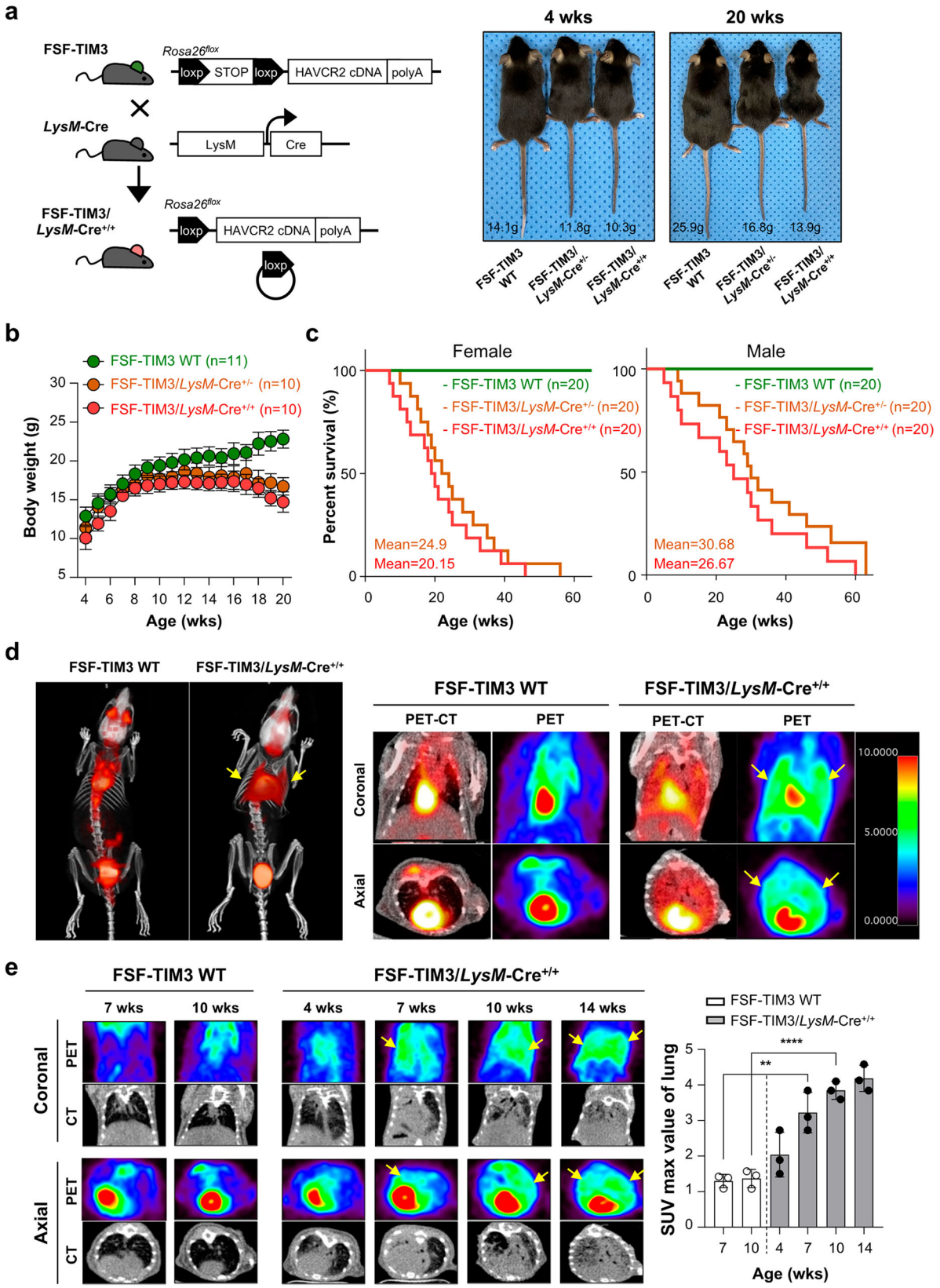

histological findings, the transcript levels of the inflammation-associated cytokines such as IL-1β, IL-10, and IL-13 were significantly elevated in FSF-TIM3/*LysM*-Cre$^{+/+}$ mice compared to WT mice (Fig. 4a).

We collected bronchoalveolar lavage fluid (BALF) from FSF-TIM3/*LysM*-Cre$^{+/+}$ and WT mice and examined the influx of inflammatory cells into BALF. Wright-Giemsa staining showed that FSF-TIM3/*LysM*-Cre$^{+/+}$ mice exhibited abnormally enlarged cells in the BALF, compared with WT mice. The total counts of infiltrated cells in BALF were significantly and age-dependently increased in FSF-TIM3/*LysM*-Cre$^{+/+}$ mice compared to WT mice (Fig. 4b). In addition, ELISA analysis showed that levels of IL-1β and

Fig. 1 | Myeloid cell-specific conditional TIM-3 knock-in mice exhibit low body weight and short lifespan. a Scheme for breeding *LysM*-Cre mice containing the targeted TIM-3 locus with Rosa26 (Left). Representative gross appearances and weights of FSF-TIM3 (WT), FSF-TIM3/*LysM*-Cre$^{+/-}$ (heterozygous), and FSF-TIM3/*LysM*-Cre$^{+/+}$ (homozygous) mice at 4 and 20 weeks of age (Right). **b** Body weights of heterozygous, homozygous, and WT female mice were measured from 4 to 20 weeks of age. **c** Comparative Kaplan-Meier survival analysis of FSF-TIM3, FSF-TIM3/*LysM*-Cre$^{+/-}$, and FSF-TIM3/*LysM*-Cre$^{+/+}$ mice at the indicated ages. **d** Representative whole body [^{18}F]FDG PET/CT images of WT and FSF-TIM3/*LysM*-Cre$^{+/+}$ mice at 14 weeks of age. Mice were administrated 18.5 MBq of [^{18}F]FDG via tail vein injection for detection of glucose metabolism. PET/CT images were obtained at 5 min after tracer injection. Yellow arrows indicate high [^{18}F]FDG uptake in the lung areas of the PET/CT scans. **e** Axial and coronal CT images and their corresponding PET images showing high [^{18}F]FDG uptake (yellow arrows) in lung areas at the indicated ages ($n = 3$ per group). Images were acquired using the OsiriX MD software. Graphs show the mean ± SD and the data were analyzed by one-way ANOVA with Tukey's multiple comparison test. $^{**}P < 0.01$ and $^{****}P < 0.0001$. Data shown are representative of three independent experiments.

TNF in the BALF were considerably higher in FSF-TIM3/*LysM*-Cre$^{+/-}$ mice than in WT mice (Fig. 4c).

Next, using flow cytometry, we quantified the innate immune cell types in the BALF from FSF-TIM3/*LysM*-Cre$^{+/-}$ and WT (Supplementary Fig. 5). As shown in Fig. 4d, the number of innate immune cells gradually increased with age in the BALF of FSF-TIM3/*LysM*-Cre$^{+/-}$ mice. No increase in innate immune cells was observed in the WT mice. To determine the inflammatory status of the accumulated myeloid cells, we examined the expression level of CD11b in the alveolar macrophages from BALF of FSF-TIM3/*LysM*-Cre$^{+/-}$ mice, since activated alveolar macrophages have been shown to express high levels of CD11b[36]. Consistent with the above findings, the CD11b expression of alveolar macrophages increased significantly with the age of FSF-TIM3/*LysM*-Cre$^{+/-}$ mice (Fig. 4e). To further evaluate the above results, we next examined the composition of immune cells in the bone marrow, spleen, and blood from WT and FSF-TIM3/*LysM*-Cre$^{+/-}$ mice. As shown in Supplementary Fig. 6a, b, we did not observe significant differences in the counts of immune cell populations in the bone marrow and spleen of FSF-TIM3/*LysM*-Cre$^{+/-}$ mice compared to WT mice. Additionally, no significant differences were observed in the immune cell composition of the blood between WT and FSF-TIM3/*LysM*-Cre$^{+/-}$ mice (Supplementary Fig. 6c). Together, these results suggest that lung abnormalities contribute to the phenotype and reduced survival of FSF-TIM3/*LysM*-Cre$^{+/-}$ mice.

Galectin-3 levels are markedly higher in the lungs of FSF-TIM3/*LysM*-Cre^{+} compared to WT mice

To understand how myeloid cell-expressed TIM-3 affects lung inflammation, we performed bulk RNA-sequencing (RNA-seq) analysis of whole lungs from FSF-TIM3/*LysM*-Cre$^{+/-}$ and FSF-TIM3 WT mice (Supplementary Fig. 7a). Differential expression analysis and volcano plots were used to visualize the up- and down-regulated genes in the lungs of FSF-TIM3/*LysM*-Cre$^{+/-}$ mice. Gene Ontology (GO) analysis showed that the differentially expressed genes (DEGs) were significantly enriched in biological processes associated with immune and inflammatory responses (Supplementary Fig. 7a). Additionally, heatmap analysis highlighted the differential expression of various inflammation-associated cytokines and chemokines in the lungs of FSF-TIM3/*LysM*-Cre$^{+/-}$ mice compared to WT mice. Of note, the expression level of galectin-3 (*Lgals3*) was markedly upregulated, as illustrated in the volcano plot and heatmap (Fig. 5a, b). Among the galectin family members, both galectin-3 and galectin-1 (*Lgals1*) were up-regulated in the lungs of FSF-TIM3/*LysM*-Cre$^{+/-}$ mice compared to WT mice. Galectin-3 binding protein (*Lgals3bp*) was also enhanced in FSF-TIM3/*LysM*-Cre$^{+/-}$ mice. In contrast, galectin-4 and galectin-12 were decreased in FSF-TIM3/*LysM*-Cre$^{+/-}$ mice compared to WT mice. Interestingly, no significant differences in the levels of galectin-9, a TIM-3 ligand, were observed between FSF-TIM3/*LysM*-Cre$^{+/-}$ mice and WT mice (Fig. 5a).

To validate these results at the protein level, we performed Western blot analysis using lung tissues of 7- and 14-week-old WT and FSF-TIM3/*LysM*-Cre$^{+/+}$ mice. Consistent with the results of our RNA-seq analysis, galectin-3 protein levels were significantly higher in the lungs of FSF-TIM3/*LysM*-Cre$^{+/+}$ mice than in WT mice (Fig. 5c), and this difference was more apparent in 14-week-old mice than 7-week-old mice. Conversely, no significant changes were observed in galectin-1 and galectin-9 protein expression between FSF-TIM3/*LysM*-Cre$^{+/+}$ and WT mice (Fig. 5c and Supplementary Fig. 7b). Since galectin-3 is known to be secreted to the extracellular space under certain conditions, especially during inflammation[37], we examined its level in BALF supernatants from FSF-TIM3/*LysM*-Cre$^{+/-}$ and WT mice. Western blot and ELISA analysis showed that the level of secreted extracellular galectin-3 was significantly higher in the BALF supernatants from FSF-TIM3/*LysM*-Cre$^{+/-}$ mice compared to WT mice (Fig. 5d, e). These results strongly suggest that galectin-3 expression levels are influenced by TIM-3 in the mouse lung.

TIM-3-overexpressing myeloid cells from lungs display up-regulation of galectin-3

Using immunohistochemical analysis of lung tissues, we further determined that TIM-3-overexpressing cells from the lungs of FSF-TIM3/*LysM*-Cre$^{+/+}$ mice displayed high expression of galectin-3 (Fig. 6a). As summarized in Fig. 6b, the intensity of galectin-3 expression was significantly higher in FSF-TIM3/*LysM*-Cre$^{+/+}$ mice than in WT mice, and the proportion of TIM-3^{+}Gal-3^{+} cells was dramatically increased in the lung tissues of FSF-TIM3/*LysM*-Cre$^{+/+}$ mice compared to WT mice. Immunocytochemical analysis of BALF cells also showed that TIM-3-overexpressing cells displayed elevated expression of galectin-3 (Fig. 6c). Flow cytometry further revealed that galectin-3 expression was progressively and significantly higher in all types of myeloid cells from FSF-TIM3/*LysM*-Cre$^{+/-}$ mice compared to WT mice. As shown in Supplementary Fig. 8a–c, the increased expression of galectin-3 is not apparent at 7 weeks, but became evident at 10 weeks and was more noticeable at 14 weeks in all types of myeloid cells we examined. ELISA analysis showed that secreted galectin-3 was markedly elevated in BALF cells from FSF-TIM3/*LysM*-Cre$^{+/-}$ mice compared to WT mice (Fig. 6d). In addition, galectin-3 expression in alveolar macrophages from FSF-TIM3/*LysM*-Cre$^{+/-}$ mice gradually increased with age and the degree of lung abnormality (Fig. 6e, f). We further investigated whether TIM-3-overexpressing alveolar macrophages exhibit inflammatory properties compared to those from WT mice by examining the expression levels of inflammation-associated cytokines using RT-PCR. The transcript levels of IL-1β, IL-6, TNF-α, and IFN-γ were significantly elevated in the alveolar macrophages of FSF-TIM3/*LysM*-Cre$^{+/-}$ mice compared to those from WT mice (Fig. 6g and Supplementary Fig. 8d).

Using FSF-TIM3$^{+/-}$/*Cx3cr1*-Cre$^{+/-}$ mice, in which TIM-3 is overexpressed in myeloid cells in the lungs, we further confirmed the up-regulation of galectin-3 in TIM-3 overexpressing myeloid cells, including alveolar macrophages, interstitial macrophages, monocytes, neutrophils, and eosinophils (Supplementary Fig. 9a–d). Galectin-3 expression increased in all types of myeloid cells from FSF-TIM3$^{+/-}$/*Cx3cr1*-Cre$^{+/-}$ mice, similar to the results obtained in FSF-TIM3/*LysM*-Cre$^{+/-}$ mice. This increased galectin-3 expression was more evident at 7 weeks of age than at 4 weeks of age. Next, we investigated the levels of galectin-3 on myeloid cells from the spleen and lymph nodes of FSF-TIM3/*LysM*-Cre$^{+/-}$ and WT mice. As shown in Supplementary Fig. 10, no significant differences in galectin-3 expression were observed between FSF-TIM3/*LysM*-Cre$^{+/-}$ and WT mice at 4 and 14 weeks of age. However, at 18 weeks of age, when FSF-TIM3/*LysM*-Cre$^{+/-}$ mice displayed strong signs of inflammation, galectin-3 levels were significantly higher in all examined myeloid cells from both the spleen and lymph nodes in FSF-TIM3/*LysM*-Cre$^{+/-}$ mice compared to those in FSF-TIM3 WT mice. Collectively, these results further support the notion that there is a link between TIM-3 and galectin-3, and suggest that galectin-3 may contribute to mediating TIM-3-associated inflammatory events in myeloid cells.

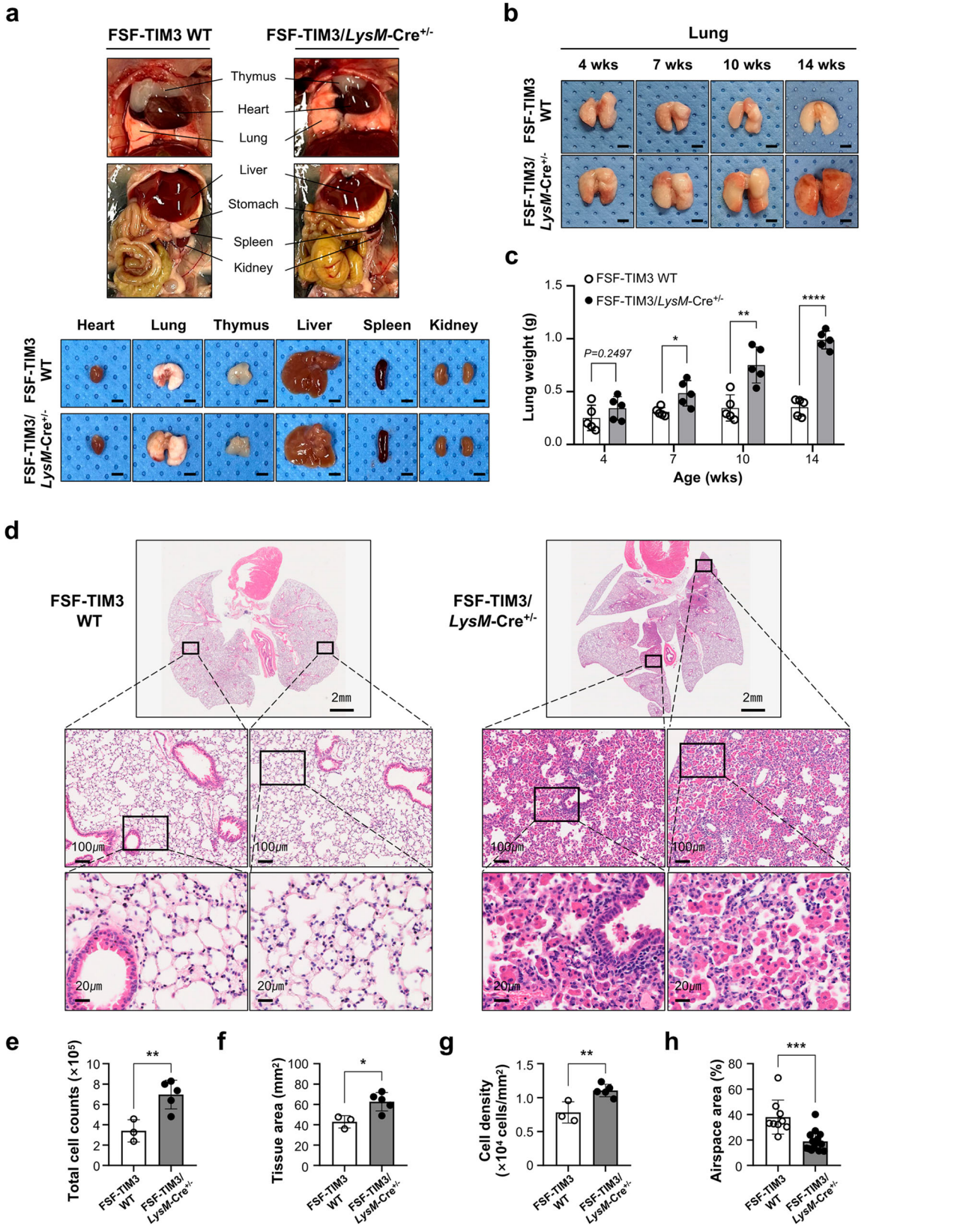

TIM-3 blockade ameliorates inflammation and galectin-3 up-regulation in the lungs of FSF-TIM3/*LysM*-Cre$^{+/-}$ mice

Next, we questioned whether blocking of TIM-3 could affect the characteristic pulmonary abnormalities of FSF-TIM3/*LysM*-Cre$^{+/-}$ mice. Accordingly, we performed pathophysiological assessment of lungs from FSF-TIM3/*LysM*-Cre$^{+/-}$ mice treated with a TIM-3-blocking antibody or control IgG every 3 days from 4 to 8 or 12 weeks of age (Fig. 7a). As shown in Fig. 7b, we observed significant decreases in some signs of inflammation, including lung weights, in 12-week-old FSF-TIM3/*LysM*-Cre$^{+/-}$ mice that had been treated with the TIM-3-blocking antibody for 8 weeks, compared

Fig. 2 | Mice with conditional overexpression of TIM-3 in myeloid cells show signs of inflammation in the lungs. a Mice were euthanized and placed in a typical ventral-side up position for necropsy at 5-week-old. Initial images present the internal regional anatomy with the abdomen open and the rib cage removed. Representative PBS-perfused images of major thoracic organs, including the heart, lungs, and thymus, as well as abdominal organs, including the liver, spleen, and kidney were obtained from WT and FSF-TIM3/*LysM*-Cre$^{+/-}$ mice. **b** Representative images of lungs from FSF-TIM3 (WT) and FSF-TIM3/*LysM*-Cre$^{+/-}$ (heterozygous) mice at the indicated weeks of age. **c** Lung weights of FSF-TIM3 and FSF-TIM3/*LysM*-Cre$^{+/-}$ mice were measured at the indicated ages ($n = 5$ per group). **d** Representative images of H&E-stained lung sections from 7-week-old FSF-TIM3 and FSF-TIM3/*LysM*-Cre$^{+/-}$ mice. **e**–**h** Quantitative analysis of total cell numbers (**e**), tissue area (**f**), cell density (**g**), and airspace area (**h**) ($n = 3$ for WT, $n = 5$ for FSF-TIM3/*LysM*-Cre$^{+/-}$). Quantification of H&E staining images was performed using the InForm2.2.1 software. At least three sections from each slide were quantified. Graphs show the mean ± SD and were analyzed by unpaired two-tailed Student's t-test. $^{*}P < 0.05$, $^{**}P < 0.01$, and $^{***}P < 0.001$.

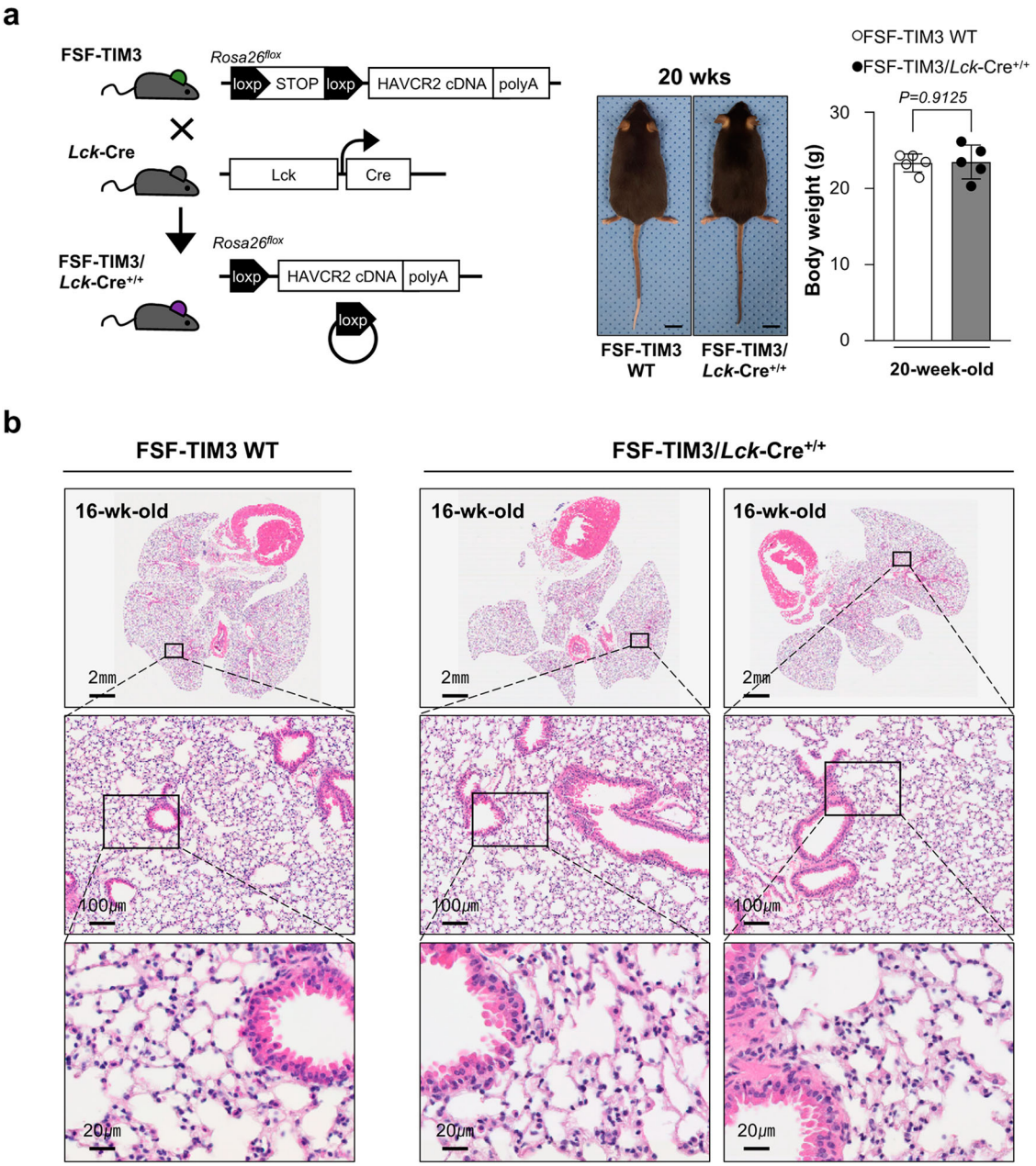

Fig. 3 | Histopathological examination of FSF-TIM3/*Lck*-Cre$^{+/+}$ mice. a Scheme for breeding *Lck*-Cre mice containing the targeted TIM-3 locus with Rosa26 (Left). Representative gross appearances and weights of FSF-TIM3 (WT), FSF-TIM3/*Lck*-Cre$^{+/+}$ (homozygous) mice at 20 weeks of age (Right). **b** Representative images of H&E-stained lung sections from FSF-TIM3 and FSF-TIM3/*Lck*-Cre$^{+/+}$ mice at 16-week-old. Quantitative analysis of total cell numbers of H&E staining images was performed using the InForm2.2.1 software. Graphs show the mean ± SD and the data were analyzed by unpaired two-tailed Student's t test.

to those with IgG for the same period. Histopathological examination under H&E staining also revealed that signs of inflammation, such as immune cell infiltration, were apparently decreased by TIM-3-blocking antibody treatment of FSF-TIM3/*LysM*-Cre$^{+/-}$ mice at 12 weeks (Fig. 7c). These results demonstrate that the TIM-3-blocking antibody ameliorates the lung abnormalities in FSF-TIM3/*LysM*-Cre$^{+/-}$ mice.

We then asked whether TIM-3 blockade could affect the level of galectin-3 in FSF-TIM3/*LysM*-Cre$^{+/-}$ mice. Galectin-3 expression was

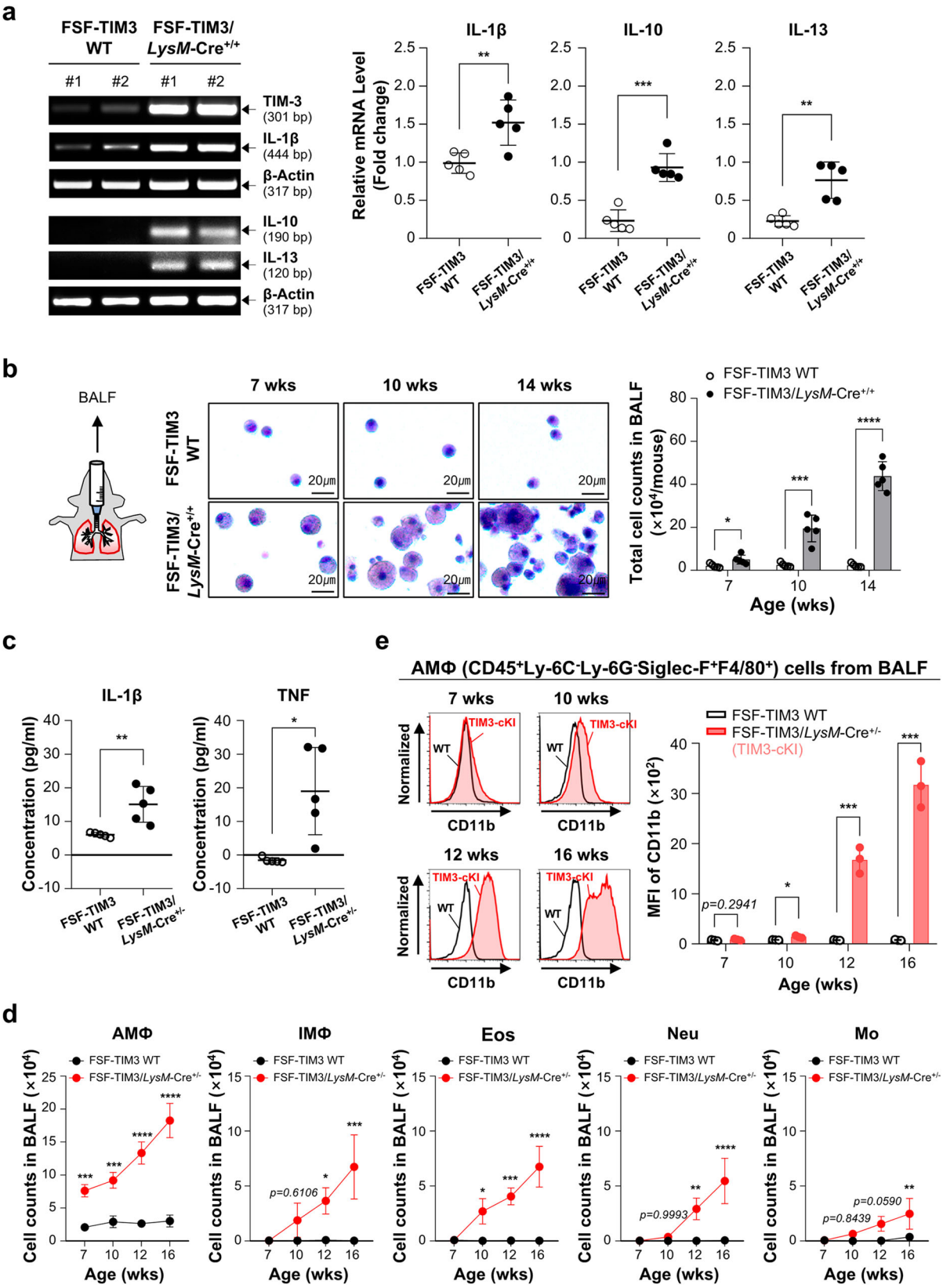

significantly lower in lung tissues from 8- or 12-week-old FSF-TIM3/*LysM*-Cre$^{+/-}$ mice treated with TIM-3-blocking antibody for 4 or 8 weeks, respectively, compared to those treated with control IgG (Fig. 7d). The effects of TIM-3 blockade on galectin-3 protein levels were more pronounced on 12-week-old FSF-TIM3/*LysM*-Cre$^{+/-}$ mice than at 8-week-old mice. To further confirm these results, we used flow cytometric analysis to examine galectin-3 expression in lung cells from FSF-TIM3/*LysM*-Cre$^{+/-}$ mice treated with TIM-3-blocking antibody or IgG. Galectin-3 levels were markedly reduced by the TIM-3-blocking antibody in all examined cell typess (Fig. 7e). Collectively, these results indicate that blockade of TIM-3

Fig. 4 | Inflammation-associated immune cells are abundant in the lungs and BALF of myeloid cell-specific TIM-3 knock-in mice. a Relative transcript levels of representative inflammation-associated cytokines were determined by RT-PCR in lung tissues of 14-week-old WT and FSF-TIM3/*LysM*-Cre$^{+/+}$ mice ($n = 5$ per group). **b** Bronchoalveolar lavage fluid (BALF) cells were collected from WT, FSF-TIM3/*LysM*-Cre$^{+/-}$ and FSF-TIM3/*LysM*-Cre$^{+/+}$ mice at the indicated time points. Representative Wright-Giemsa staining images showing the cell morphology (original magnification of 40×) of BALF cells from WT and FSF-TIM3/*LysM*-Cre$^{+/+}$ mice. Bar graph shows the total cell counts in the BALF ($n = 5$ per group). **c** ELISA of IL-1β and TNF-α expression in BALF from 14-week-old mice. Graphs show the mean ± SD and were analyzed by unpaired two-tailed Student's t test. $^{*}P < 0.05$, $^{**}P < 0.01$, $^{***}P < 0.001$, and $^{****}P < 0.0001$. The data presented are representative of three independent experiments. **d** Cell counts of myeloid innate immune cells in BALF from the WT and FSF-TIM3/*LysM*-Cre$^{+/-}$ mice, as determined by flow cytometry (AMΦ, alveolar macrophage; IMΦ, interstitial macrophage; Eos, eosinophil; Neu, neutrophil; Mo, monocyte, $n = 3$ per group). **e** CD11b expression levels in alveolar macrophages (AMΦ, CD45^{+}Ly6C^{-}Ly6G^{-}SiglecF^{+}F4/80^{+}) from BALF were examined by flow cytometry using FACS verse. Graphs show the mean ± SD and were analyzed by one-way ANOVA with Tukey's multiple comparison test. $^{*}P < 0.05$, $^{**}P < 0.01$, $^{***}P < 0.001$, and $^{****}P < 0.0001$.

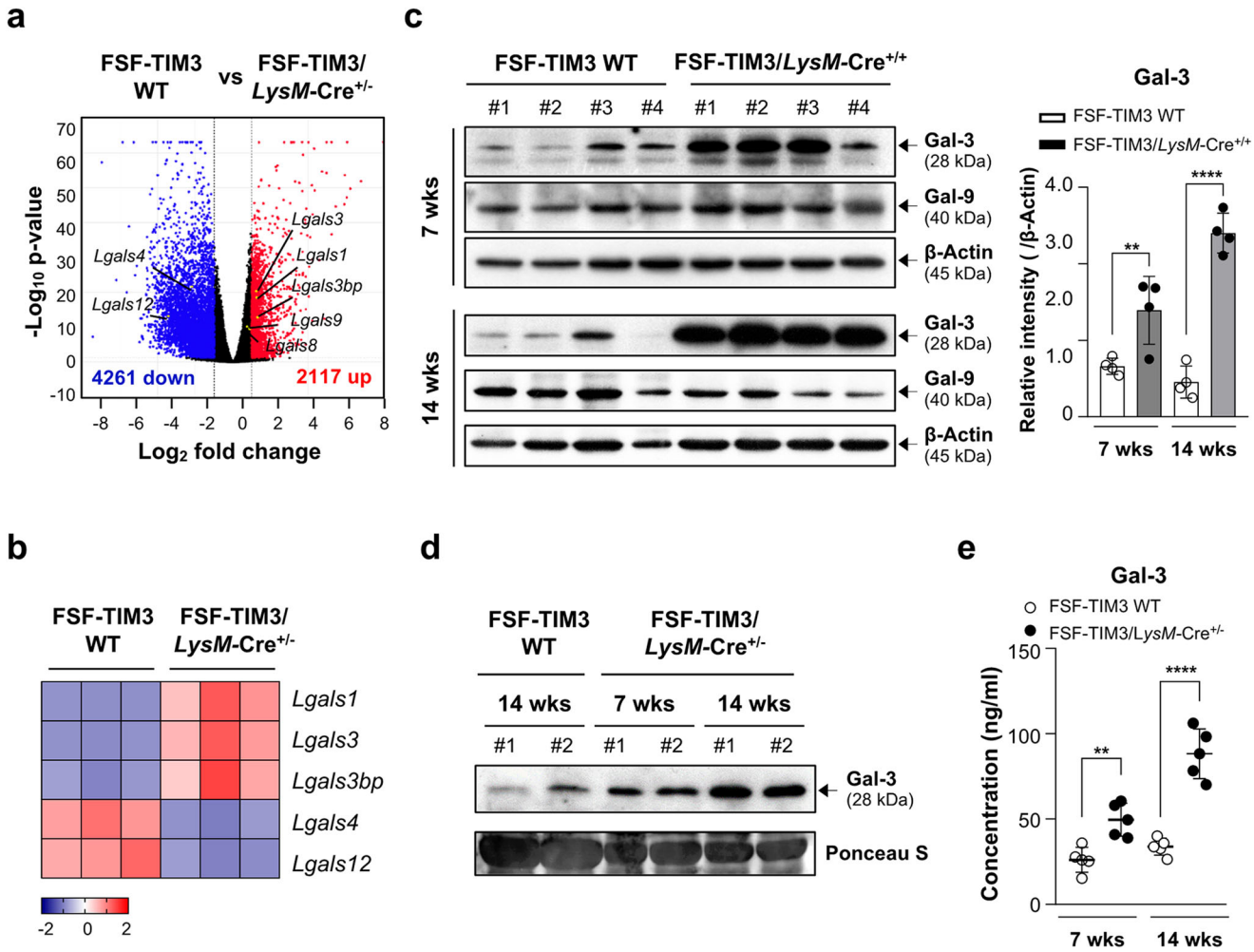

Fig. 5 | Galectin-3 levels are markedly higher in the lungs of myeloid cell-specific TIM-3 knock-in mice compared to WT mice. a Bulk RNA-sequencing data obtained from whole lungs of FSF-TIM3 (WT) and FSF-TIM3/*LysM*-Cre$^{+/-}$ mice, visualized with a Volcano plot highlighting differentially expressed genes (DEGs) ($n = 3$ per group, $\log_2FC \geq 2$, $P < 0.05$). **b** Heatmap showing the expression of galectins and galectin-binding protein. Data shown are relative to the Z-scores calculated across the samples. Red indicates relatively high levels of expression; blue indicates relatively low levels of expression. **c** Protein extracts were obtained from the lung tissues of WT and FSF-TIM3/*LysM*-Cre$^{+/+}$ mice at 7 and 14 weeks of age. The samples were subjected to western blot analysis with the indicated antibodies. d Western blot analysis was carried out on BALF supernatants with an anti-galectin-3 antibody. **e** ELISA was performed to assess the concentration of galectin-3 in BALF ($n = 5$ per group). Graphs show the mean ± SD and the data were analyzed by two-way ANOVA with Sidak's multiple comparison test. $^{**}P < 0.01$ and $^{****}P < 0.0001$.

reduces lung abnormalities and galectin-3 expression in myeloid cell-specific TIM-3 knock-in mice.

Administration of the galectin-3 inhibitor GB1107 reduces inflammation in FSF-TIM3/*LysM*-Cre$^{+/-}$ mice

To validate the above results, we investigated whether inhibition of galectin-3 could affect inflammatory events in the lungs of FSF-TIM3/*LysM*-Cre$^{+/-}$ mice using GB1107, a galectin-3 inhibitor that binds specifically to its carbohydrate-recognition domain[38]. FSF-TIM3/*LysM*-Cre$^{+/-}$ mice were treated with intraperitoneal injection of GB1107 or vehicle every 2 days from 7 to 10 weeks of age (Fig. 8a). The lungs of GB1107-treated mice had fewer external signs of inflammation and weighed less than the lungs of vehicle-treated mice (Fig. 8b). Histopathological examination revealed that GB1107-treated FSF-TIM3/*LysM*-Cre$^{+/-}$ mice had reduced disease-related features compared to vehicle-treated mice. Specifically, there were

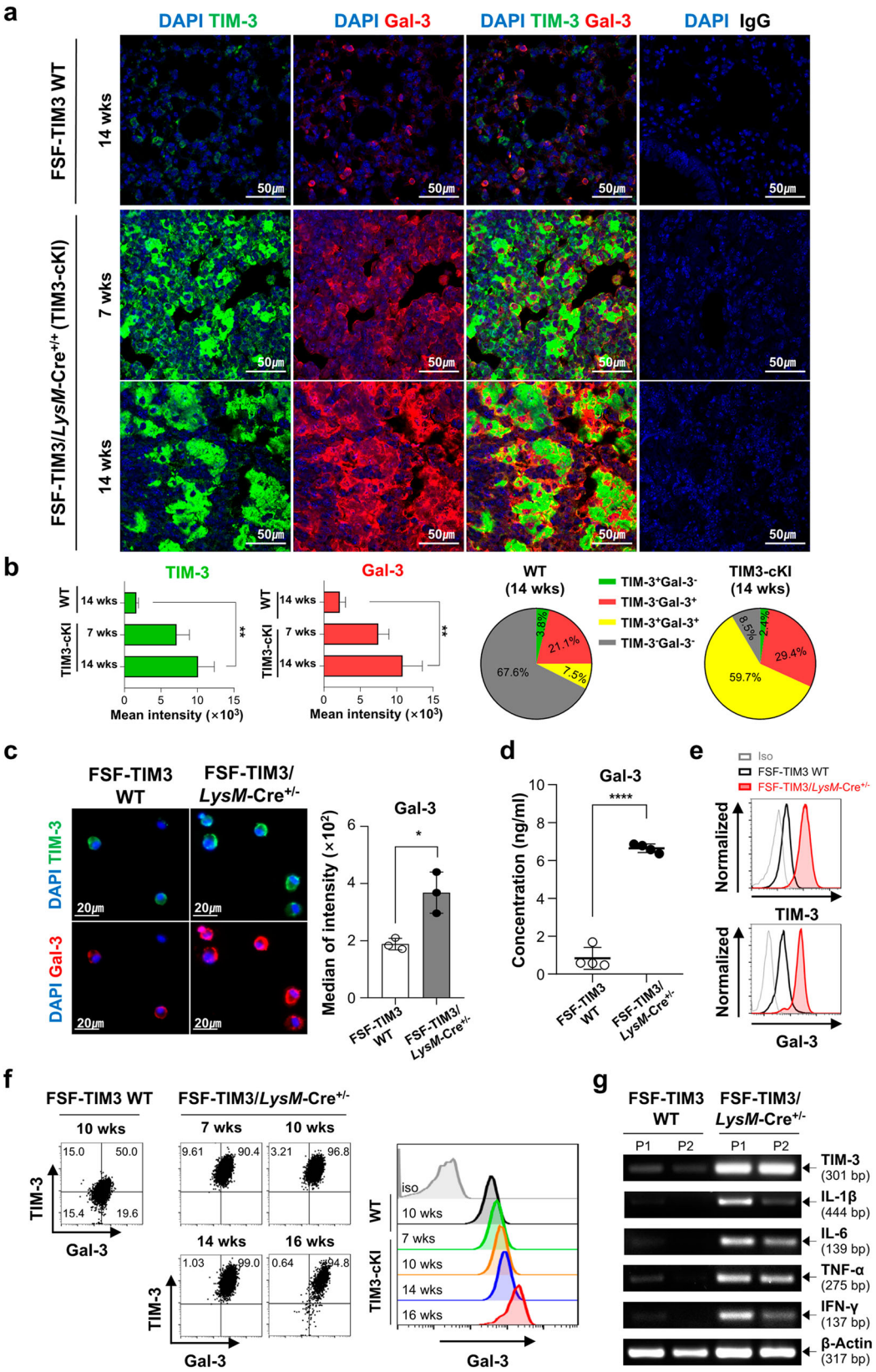

fewer cell infiltrates, reduced tissue area and cell density, and increased airspace area in the lungs of GB1107-treated FSF-TIM3/*LysM*-Cre$^{+/-}$ mice (Fig. 8c–g). Consistent with the histopathologic examination, the transcript levels of IL-1β and TNF-α were significantly reduced in lung tissues of GB1107-treated mice compared to vehicle-treated mice (Fig. 8h). Collectively, these results provide that galectin-3 inhibition reduces lung inflammation in myeloid cell-specific TIM-3 knock-in mice.

Fig. 6 | Galectin-3 levels are enhanced in TIM-3-overexpressing myeloid cells from the lungs. a Representative immunohistochemical images of lung tissues obtained from WT and FSF-TIM3/*LysM*-Cre$^{+/+}$ mice using the indicated antibodies ($n = 3$ per group). **b** The relative and mean intensities were quantified using the Zen software. Graphs show the mean ± SD and the data were analyzed by one-way ANOVA with Tukey's multiple comparison test. $^{**}P < 0.01$. **c** BALF was isolated from 4-week-old WT and FSF-TIM3/*LysM*-Cre$^{+/-}$ mice ($n = 3$ per group). Immunocytochemical analysis of BALF cells was performed using antibodies against TIM-3 (green) and galectin-3 (red), with nuclei counterstaining (DAPI). Quantification of mean fluorescence intensity was performed using the Zen software. **d** ELISA was applied to detect the concentration of galectin-3 in serum-free media of cultured BALF cells obtained from 4-week-old mice ($n = 4$ per group). **e** Flow cytometric analysis of TIM-3 and galectin-3 in AMΦ cells from BALF of 4-week-old mice. **f** Representative dot plots and histogram of TIM-3 and galectin-3 in AMΦ cells from lung tissues obtained from WT and FSF-TIM3/*LysM*-Cre$^{+/-}$ mice of the indicated age ($n = 4$ per group). **g** Relative transcript levels of representative inflammation-associated cytokines were determined by RT-PCR in AMΦ cells sorted from the lungs of 4-week-old WT and FSF-TIM3/*LysM*-Cre$^{+/-}$ mice. AMΦ cells were sorted from four mice and pooled into one sample (P). Graphs shows the mean ± SD and the data were analyzed by unpaired two-tailed Student's t test. $^{*}P < 0.05$ and $^{****}P < 0.0001$.

LPS-induced lung inflammation is significantly decreased in TIM3$^{f/f}$/*LysM*-Cre$^{+/+}$ mice compared to WT mice

To further validate the association of TIM-3 on myeloid cells with lung inflammation, we assessed the impact of myeloid cell-specific knock-out on lung inflammation. For this, we established a floxed TIM-3 (TIM3$^{f/f}$) mouse strain and bred these mice with *LysM*-Cre mice (Fig. 9a). TIM3$^{f/f}$/*LysM*-Cre$^{+/+}$ and TIM3$^{f/f}$ mice were intranasally injected with LPS (10 μg in 30 μl) or PBS at the indicated time points to generate a pulmonary inflammation model (Fig. 9b). The lung tissues were stained with H&E and then scored blindly according to a histological scoring system[39,40] (Supplementary Fig. 11). Figure 9c, d show that LPS-induced lung inflammation was significantly decreased in the lungs of TIM3$^{f/f}$/*LysM*-Cre$^{+/+}$ mice compared to WT mice. To confirm these findings, we examined the mRNA levels of TNF-α and IL-1β in lung tissues by quantitative RT-PCR analysis. The transcript levels of IL-1β and TNF-α were markedly elevated in LPS-injected TIM3$^{f/f}$ mice and were significantly less elevated in LPS-injected TIM3$^{f/f}$/*LysM*-Cre$^{+/+}$ mice (Fig. 9e).

We next investigated whether the galectin-3 expression was altered by LPS injection and, if so, whether the extent of this change was affected by the absence of TIM-3 on myeloid cells. Galectin-3 expression was significantly elevated in alveolar macrophages, interstitial macrophages, monocytes, and neutrophils from the lungs of WT mice at 72 h after LPS injection, but these changes were significantly reduced in the corresponding cells from LPS-injected TIM3$^{f/f}$/*LysM*-Cre$^{+/+}$ mice (Fig. 9f). We further examined whether galectin-3 inhibition could affect the LPS-induced inflammation in myeloid cells using GB1107. Bone marrow-derived macrophages were treated with 100 ng/ml LPS along with either vehicle or the indicated concentrations of GB1107 for 24 h, and levels of iNOS and IFN-γ, representative inflammatory mediators, were determined by flow cytometry. LPS treatment elevated the expression of iNOS and IFN-γ, which was significantly reduced by treatment with GB1107 (Supplementary Fig. 12). Together, these findings underscore the involvement of TIM-3 on myeloid cells in modulating galectin-3 levels and lung inflammation, suggesting a link between galectin-3 and LPS-induced inflammation in myeloid cells.

Discussion

Lung inflammation is a hallmark of most lung diseases, including acute lung injury, viral infectious pulmonary diseases, chronic airway pulmonary disease, and lung cancer[15,41]. It is a natural protective response to harmful stimuli, such as pathogens, damaged cells, and toxic agents. However, inappropriate inflammation and unresolved lung injury can cause gas exchange impairment and diverse diseases in the lungs. Thus, clinicians and researchers have earnestly sought to understand the detailed molecular mechanisms underlying disease-associated lung inflammation. In this study, while conducting investigations using myeloid cell-specific TIM-3 conditional knock-in and knock-out mice, we have obtained novel interesting findings regarding the function of TIM-3 on myeloid cells in the lungs and uncover a possible mechanism underlying the TIM-3-mediated lung inflammation.

TIM-3 has been reported to have distinct characteristics according to the context and/or cell type[10,34,35]. We previously reported that TIM-3 on myeloid cells has expressional patterns and functions distinct from those of TIM-3 on T cells[6,7]. To further explore the cell-specific and context-dependent nature of TIM-3, we generated conditional myeloid cell-specific TIM-3 knock-in and knock-out mice. Both heterozygous FSF-TIM3/*LysM*-Cre$^{+/-}$ and homozygous FSF-TIM3/*LysM*-Cre$^{+/+}$ mice showed dramatic changes in appearances, with small size and low body weight as well as poor survival and shorter median survival times, compared to FSF-TIM3 mice (Fig. 1). Moreover, diagnostic whole-body PET/CT imaging and histopathological examination strongly suggested that myeloid cell-specific overexpression of TIM-3 led to severe inflammatory abnormalities in the lungs (Fig. 2). Several previous reports indicated that TIM-3 may be associated with lung abnormality, but these studies did not focus on the specific functions/importance of TIM-3 in myeloid cells. Wang et al. reported that when bleomycin was used to induce lung fibrosis, TIM-3 transgenic mice developed more serious pathological changes than WT mice[42]. In addition, TIM-3 levels on T cells were reported to be elevated in patients with *M.tuberculosis*-induced tuberculosis and nontuberculous mycobacterial lung disease[43,44]. Collectively, our results and the previous findings suggest that TIM-3 on myeloid cells mediates inflammatory responses in the lungs to induce lung abnormality and a disease phenotype with weight loss.

We further explored the mechanism(s) by which TIM-3 on myeloid cells contributes to disease-associated lung inflammation and found that galectin-3 was elevated in the lung tissues and BALF of FSF-TIM3/*LysM*-Cre$^{+/-}$ mice compared to WT mice. Accumulating data indicate that galectin-3 contributes to chronic and acute pulmonary diseases in patients and mice[45–47]. In particular, expressional changes of galectin-3 are reported to contribute to the pathogenesis of pulmonary diseases, including COPD, asthma, and fungal infection[25,48,49]. In addition, inhibition of galectin-3 ameliorated inflammation-associated lung diseases and LPS-induced lung injury[47]. For example, conditional myeloid deletion of galectin-3 developed less severe inflammation in Avian H5N1 Influenza A Virus-induced pulmonary model[50]. Hirani et al. reported that administration of TD139, a galectin-3 inhibitor, showed not only reduction of galectin-3 levels in alveolar macrophages and decrease of plasma biomarkers associated with IPF in an IIPF clinical study[51]. Additionally, recent studies suggested that galectin-3 has potential role in the inflammation and pulmonary diseases associated with Covid-19 infection[52–54]. Based on these reports and our present results, we speculate that TIM-3 affects the level and function of galectin-3, thereby leading to characteristic inflammatory status of lungs and health condition in FSF-TIM3/*LysM*-Cre^{+} mice.

Our results convincingly support that TIM-3 on myeloid cells critically modulates lung inflammation and lead us to propose that galectin-3 could mediate TIM-3-associated inflammatory events. Galectin-3 was highly expressed in all types of TIM-3-overexpressing myeloid cells from FSF-TIM3/*LysM*-Cre$^{+/-}$ and FSF-TIM3/*LysM*-Cre$^{+/+}$ mice, including alveolar macrophages, interstitial macrophages, neutrophils, monocytes, and eosinophils. Additionally, we found that galectin-3 expression was higher in myeloid cells from FSF-TIM3$^{+/-}$/*Cx3cr1*-Cre$^{+/-}$ mice, in which TIM-3 is overexpressed in the lungs, compared to those from WT mice (Supplementary Fig. 9). Although FSF-TIM3$^{+/-}$/*Cx3cr1*-Cre$^{+/-}$ mice display high TIM-3 expression not only in CD11b^{+} myeloid cells but also in other cells, including CD3^{+} T cells, due to the leakiness of Cre activity, our results support the association of galectin-3 expression with TIM-3 expression.

Myeloid cells make up a large proportion of the inflammatory lung microenvironment, where they interact with structural cells and centrally

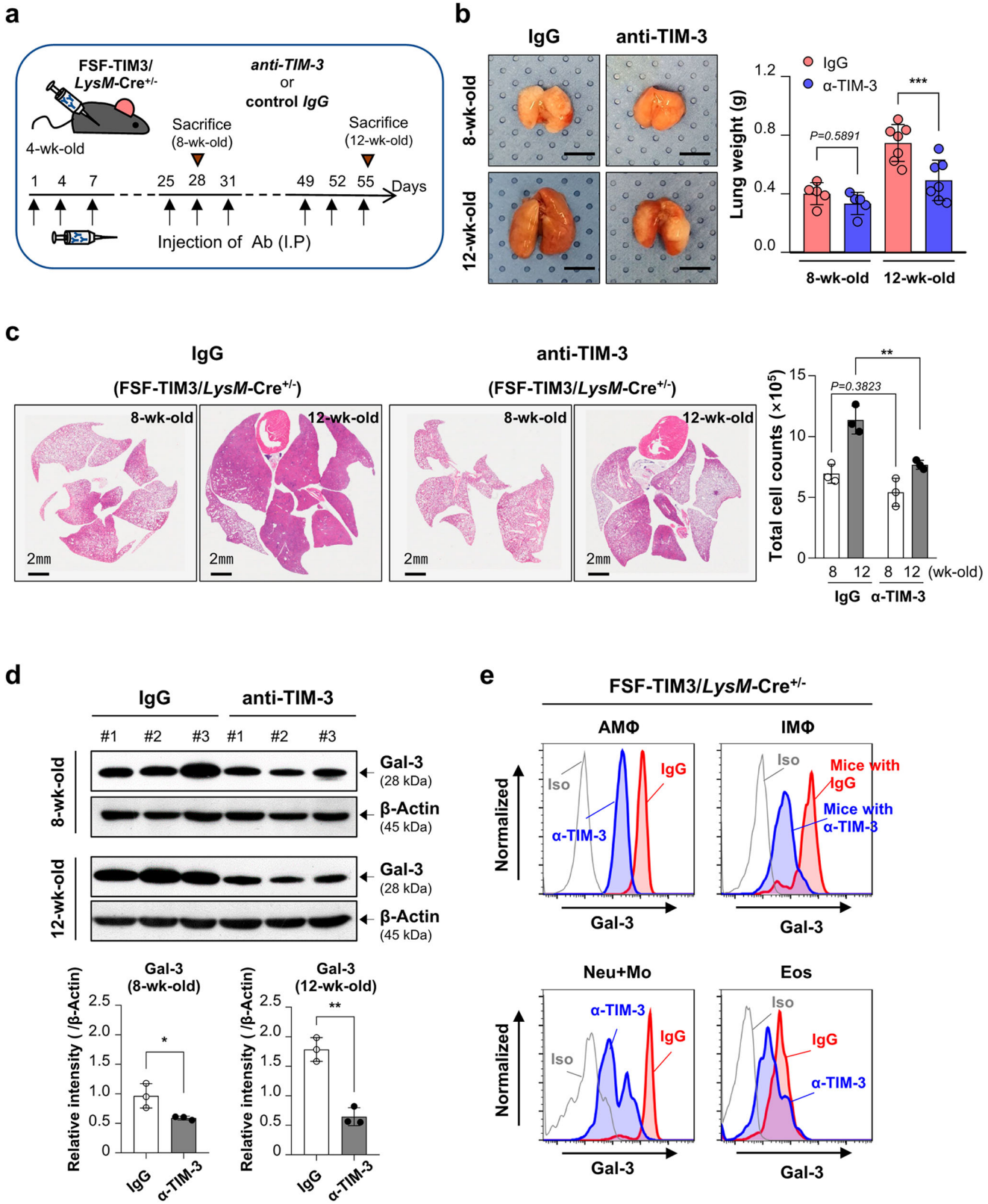

contribute to innate and adaptive immunity by producing inflammatory mediators[14]. Galectin-3, like other cytokines and inflammatory mediators, is expressed in myeloid cells (e.g., macrophages) and contributes to the functions of myeloid cells under pathophysiological conditions. Multiple functions of galectin-3 have been reported to be largely attributed to its CRD. The CRD of galectin-3 may interact with immune and inflammation-associated molecules, including a variety of glycan-containing molecules on diverse cell surfaces and within the extracellular matrix[46,55]. Although we did not pinpoint the underlying mechanism of amelioration of inflammation by GB1107, it is likely that TIM-3-associated increase of galectin-3 affects interaction with inflammation-associated molecules. Increasing studies have revealed that the expression and secretion of galectin-3 are up-regulated in

Fig. 7 | TIM-3 blockade ameliorates pulmonary abnormalities in FSF-TIM3/*LysM*-Cre$^{+/-}$ mice. a Scheme of experiments used to generate the data shown in (**b**–**e**). FSF-TIM3/*LysM*-Cre$^{+/-}$ mice were intraperitoneally treated with TIM-3-blocking antibody or control IgG (100 μg in 100 μl). ($n = 5$ for 8-week-old mice, $n = 7$ for 12-week-old mice). **b** Representative images of the lungs treated with TIM-3-blocking antibody or IgG. Lung weights are shown in the graph. **c** Representative H&E staining images of lung tissues from IgG- or TIM-3 antibody-treated FSF-TIM3/*LysM*-Cre$^{+/-}$ mice ($n = 3$ per group). Graphs show the mean ± SD and the data were analyzed by two-way ANOVA with Sidak's multiple comparison test. $^{**}P < 0.01$ and $^{***}P < 0.001$. **d** Western blot analysis was performed on lung tissues from IgG- or TIM-3 antibody-treated FSF-TIM3/*LysM*-Cre$^{+/-}$ mice using the antibodies against galectin-3 and β-Actin. Graphs show the mean ± SD and the data were analyzed by unpaired two-tailed Student's t-test. $^{*}P < 0.05$, and $^{**}P < 0.01$. **e** Cells were isolated from the lungs of 12-week-old FSF-TIM3/*LysM*-Cre$^{+/-}$ mice treated with a TIM-3-blocking antibody or control IgG, and then subjected to flow cytometry using antibodies against galectin-3 and representative marker antibodies for each cell type in the lungs.

patients and animal models of diverse disease conditions[56]. Previously, we reported that galectin-3 exerts cytokine-like regulatory actions through JAK-STAT pathway in microglia, which are brain resident innate immune cells[57]. In addition, studies have shown that galectin-3 expression is regulated by several signaling molecules, including NF-κB[58], HIF-1α, protein kinase C, Ras, MAPkinases, AP-1, HIF-1and SREBP1[59] in several types of cells including macrophages. Galectin-3 has also been reported to be induced and modulated by various inflammatory cytokines including IL-2, IL-4, TNF-α, IFN-γ and IL-7[60]. Moreover, it has been reported that TIM-3 activation affects the activity of immune and inflammatory signaling molecules such as NF-κB and PI3K/AKT[35,61]. Based on our results and previous studies, it is likely that TIM-3 and TIM-3-driven galectin-3 expression are closely involved in the inflammatory responses of the lung.

Increasing studies highlight that TIM-3 function varies, acting as either an inhibitory or stimulatory regulator based on cell type and specific conditions. In myeloid cells. Ruffell group has reported the regulatory roles of TIM-3 in classical dendritic cells (cDC) in murine models of mammary carcinoma. They showed that TIM-3 suppresses the endocytosis of extracellular dsDNA by cDCs, thereby preventing the activation of cGAS-STING pathway, the expression of type I IFNs, and the production of CXCL9 or CXCL10[62]. Recently, they reported that anti-TIM-3 antibody improved the response to paclitaxel chemotherapy by affecting intratumoral CD103^{+} cDCs in models of triple-negative and luminal B disease[63]. Additionally, Dixon et al. reported that TIM-3 regulates the function of DC, affecting anti-tumor immunity by increasing NLRP3 inflammasome activation[64]. In myeloid cells of the brain, Ausejo-Mauleon et al. reported that TIM-3 blockade triggers a potent immune response by converting the DIPG tumor microenvironment to a proinflammatory phenotype through microglia[65]. Previously, we found that the expression and function of microglial TIM-3 differ between an intracranial orthotopic mouse glioma model and the Hypoxia/Ischemia model[66]. Moreover, TIM-3 expression patterns were distinct between T cells and myeloid cells in the brain tumor microenvironment[7]. Together, our findings and those of others suggest that TIM-3 responds distinctively to certain conditions, mediating specific immune responses in a context-dependent manner.

Gayden et al. reported that patients with germline loss-of-function mutations, lacking surface TIM-3 expression, suffer from severe autoimmune phenotypes with macrophage hyperactivation[67]. In contrast, we found severe pulmonary inflammation in myeloid-specific TIM-3 conditional knock-in mice, but not evident in T cell-specific TIM-3 knock-in mice. These findings underscore the importance of TIM-3 in myeloid cells and its potential as a therapeutic target. Kearley et al. reported that blocking TIM-3 function improved pulmonary inflammation by skewing the Th2 response to Th1 in allergen-induced airway inflammation[66]. Jayaraman et al. found that TIM-3 blockade reduced *M. tuberculosis* burden by affecting the interaction between TIM-3 expressed on T cells and galectin-9 on macrophages[68]. A recent study indicated that TIM-3 loss on DCs reduced tumor burden in non-small-cell lung carcinoma model[64]. Conversely, TIM-3 monoclonal antibodies increased the inflammation severity in a Th1-mediated EAE model and a bleomycin-induced pulmonary fibrosis model[69,70]. Considering the differential actions of TIM-3 in specific cell types and in different contexts, therapeutic approaches targeting TIM-3 should be carefully developed with consideration of its characteristics in specific disease conditions.

In summary, our findings suggest that overexpression of TIM-3 on myeloid cells leads to cause excessive lung inflammation, which is accompanied by the accumulation of many inflammatory cells, increased production of inflammatory mediators, enlargement of lungs, and loss of weight. Our experiments with TIM-3 blockade and conditional TIM-3 knock-in and knock-out mice further show that galectin-3 is an important mediator of TIM-3-associated inflammatory events (Fig. 10). Overall, our results suggest that modulating TIM-3 and galectin-3 could benefit inflammation-associated lung diseases. This study provides new insights into the immunoregulatory activity of myeloid cell-expressed TIM-3 in the lungs. Further studies and careful interpretation of the TIM-3-galectin-3 axis could facilitate the development of novel therapeutic strategies against inflammation-associated lung diseases.

Methods

Mice

Eight-week-old male C57BL/6 mice were purchased from ORIENT BIO (Gapyeong, Korea). *LysM*-Cre mice, *Cx3cr1*-Cre mice, and *Lck*-Cre mice were obtained from The Jackson Laboratory (Bar Harbor, ME, USA). C57BL/6 mice carrying a Rosa26 knock-in of a flox-stop-flox cassette containing a Flag-tagged mTim-3 cDNA (FSF-TIM3) were generated by Dr. Lawrence P. Kane[35]. C57BL/6 J mice carrying a loxp site in exon 4 of the TIM-3 gene (TIM-3$^{f/f}$) were produced in our laboratory using an embryonic stem (ES) cell clone from the MMRRC at UC Davis in our laboratory. The ES cell clones were injected into C57BL/6 J blastocyst-stage embryos, and the injected blastocysts were surgically implanted into the uteri of pseudo pregnant surrogate mothers. All mice were maintained and bred under specific pathogen-free conditions in the Association for Assessment and Accreditation of Laboratory Animal Care–accredited animal facility of the National Cancer Center (NCC) Korea. Age-matched female mice at 4 to 20 weeks of age were used for all experiments. Both male and female mice were monitored up to 65 weeks of age for survival analysis. All animal were euthanize using Zoletil anesthesia followed by CO_2 inhalation and all procedures were performed according to ARRIVE guidelines and NCC guidelines for the care and use of laboratory animals. We have complied with all relevant ethical regulations for animal use. The protocol was approved by the Committee on the Ethics of Animal Experiments of the NCC in the animal facilities of the National Cancer Center (Permit Number: NCC-22-547, NCC-22-597, NCC-23-784). To avoid bias, the animals in this study were properly randomized with blinding for genotypes and treatments.

Animal PET/CT Imaging

All mice were fasted (given water only) for 6 h before PET/CT scans. Anesthesia was induced with 2% isoflurane/100% O_2, and 18.5 MBq of [^{18}F] FDG was intravenously injected to each mouse. The animal PET/CT system, eXplore Vista PET/CT (GE), was utilized; normalization, scatter correction and attenuation correction were applied for PET scans acquired over 5 min per bed position. The obtained images were reconstructed with iterative reconstruction (OSEM 2-D, 32 subsets, two interactions). For CT scans, the X-ray conditions were: 250 μA and 40 kV for 7 min. The CT resolution was 200 μm, and 360 projections were acquired. All image analyses were done using the OsiriX MD software (www.osirix-viewer.com, Pixmeo SARL, Switzerland).

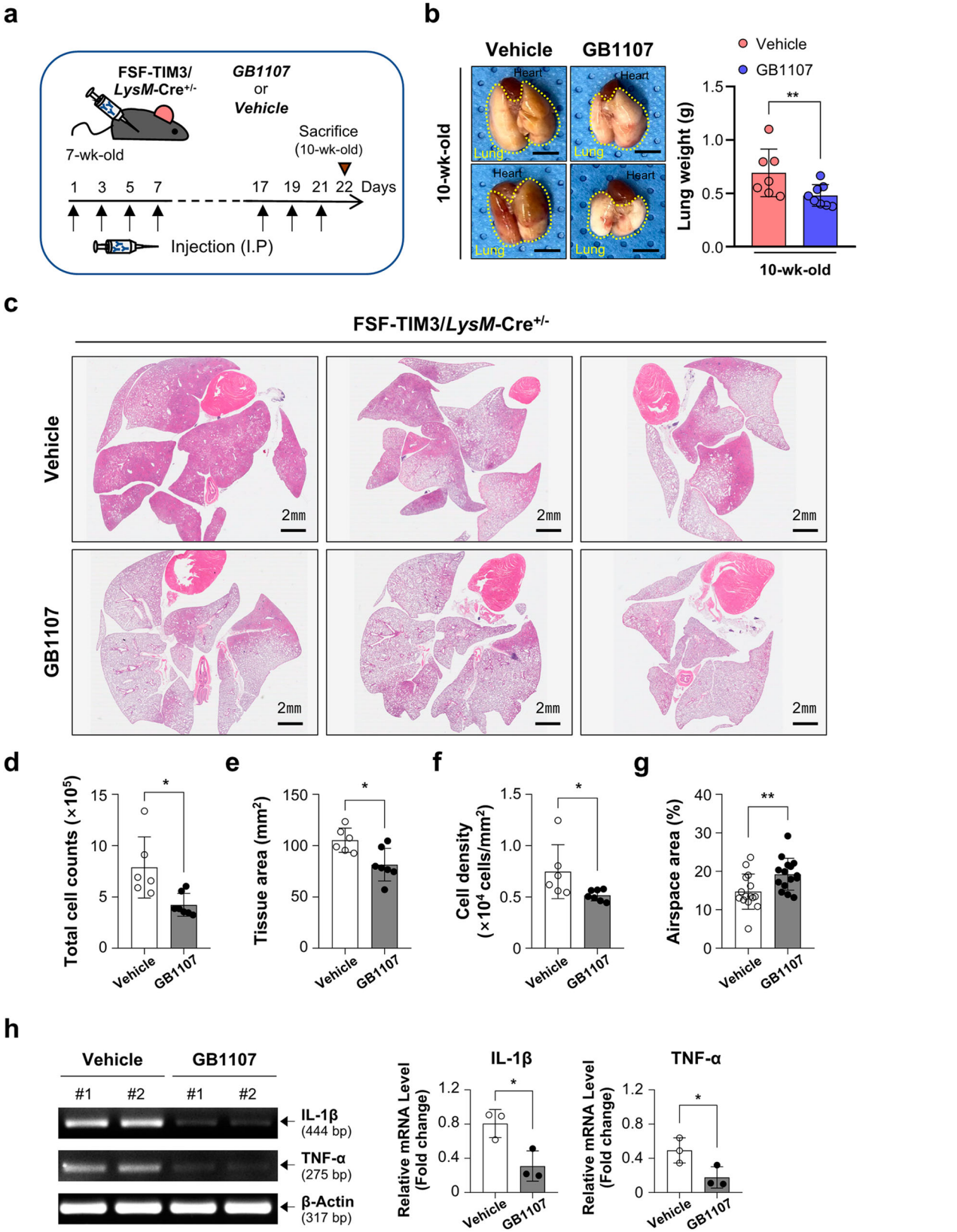

Fig. 8 | GB1107, a selective Galectin-3 inhibitor, ameliorates pulmonary abnormalities in FSF-TIM3/*LysM*-Cre$^{+/-}$ mice. a Scheme of experiments used to generate the data shown in (**b**–**h**). FSF-TIM3/*LysM*-Cre$^{+/-}$ mice were intraperitoneally treated with either GB1107 (1 mg/kg/every 2 days) or a vehicle control. **b** Representative images and weights of lungs from FSF-TIM3/*LysM*-Cre$^{+/-}$ mice treated with GB1107 or the vehicle ($n = 6$ for vehicle group, $n = 7$ for GB1107 group). **c** Representative H&E staining images of lung tissues from both vehicle- and GB1107-treated FSF-TIM3/*LysM*-Cre$^{+/-}$ mice. **d**–**g** Quantitative analysis of total cell numbers (**d**), tissue area (**e**), cell density (**f**), and airspace area (**g**) in H&E-stained lung sections. Quantification was performed using InForm2.2.1 software, with at least three sections analyzed per slide. **h** Relative transcript levels of IL-1β and TNF-α determined by RT-PCR in FSF-TIM3/*LysM*-Cre$^{+/-}$ mice ($n = 3$ per group). Data are presented as mean ± SD and were analyzed using an unpaired two-tailed Student's t-test. $^{*}P < 0.05$ and $^{**}P < 0.01$.

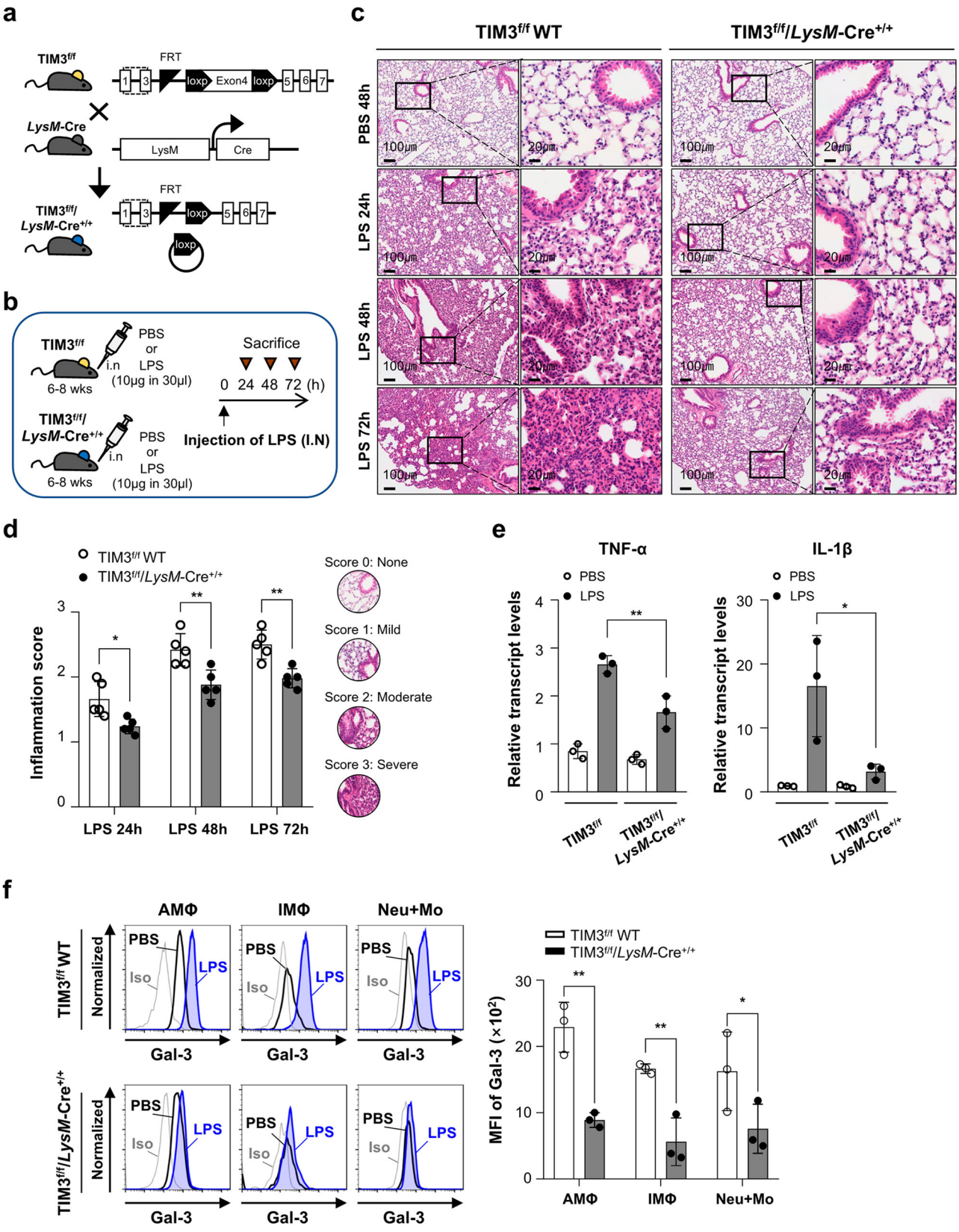

Histology of lungs

Mice were euthanized and transcardially perfused with ice-cold PBS and the lungs were harvested and immediately fixed in formalin for 24 h. After fixation, lung tissues were paraffin-embedded and sectioned at 4 μm, and the sections were stained with H&E according to standard procedures. H&E slides were imaged using a Vectra 3.0 spectral imaging system (PerkinElmer) under the brightfield protocol, and were analyzed with the InForm 2.2.1 image analysis software (PerkinElmer).

Fig. 9 | LPS-induced inflammation is decreased in myeloid-specific TIM-3 knock-out mice compared to WT mice. a Conditional myeloid-specific TIM-3 knock-out mice (TIM3$^{f/f}$/*LysM*-Cre$^{+/+}$, TIM3-cKO) were generated by crossing the TIM3$^{f/f}$ mice with *LysM*-Cre mice. **b** Schematic representation of the LPS-induced murine lung injury model used in this study; TIM3$^{f/f}$ and TIM3$^{f/f}$/*LysM*-Cre$^{+/+}$ mice were intranasally (i.n) injected with LPS (10 μg in 30 μl) or PBS and assessed after the indicated durations ($n = 3$ for PBS group, $n = 5$ for LPS group). **c** Representative H&E staining images of lung tissues from the LPS-treated mice. **d** Inflammation scores based on histological examination of lung sections ($n = 5$ per group). **e** Relative mRNA levels of TNFA and IL-1β in lung tissues of TIM3$^{f/f}$ and TIM3$^{f/f}$/*LysM*-Cre$^{+/+}$ mice at 72 h post LPS treatment were determined by qRT-PCR ($n = 3$ per group). **f** Representative histogram of galectin-3 expression in myeloid cells from lung tissues of TIM3$^{f/f}$ and TIM3$^{f/f}$/*LysM*-Cre$^{+/+}$ mice at 72 h after intranasally administration of LPS ($n = 3$ per group). Graphs show the mean ± SD and the data were analyzed by two-way ANOVA with Sidak's multiple comparison test. $^{*}P < 0.05$, $^{**}P < 0.01$.

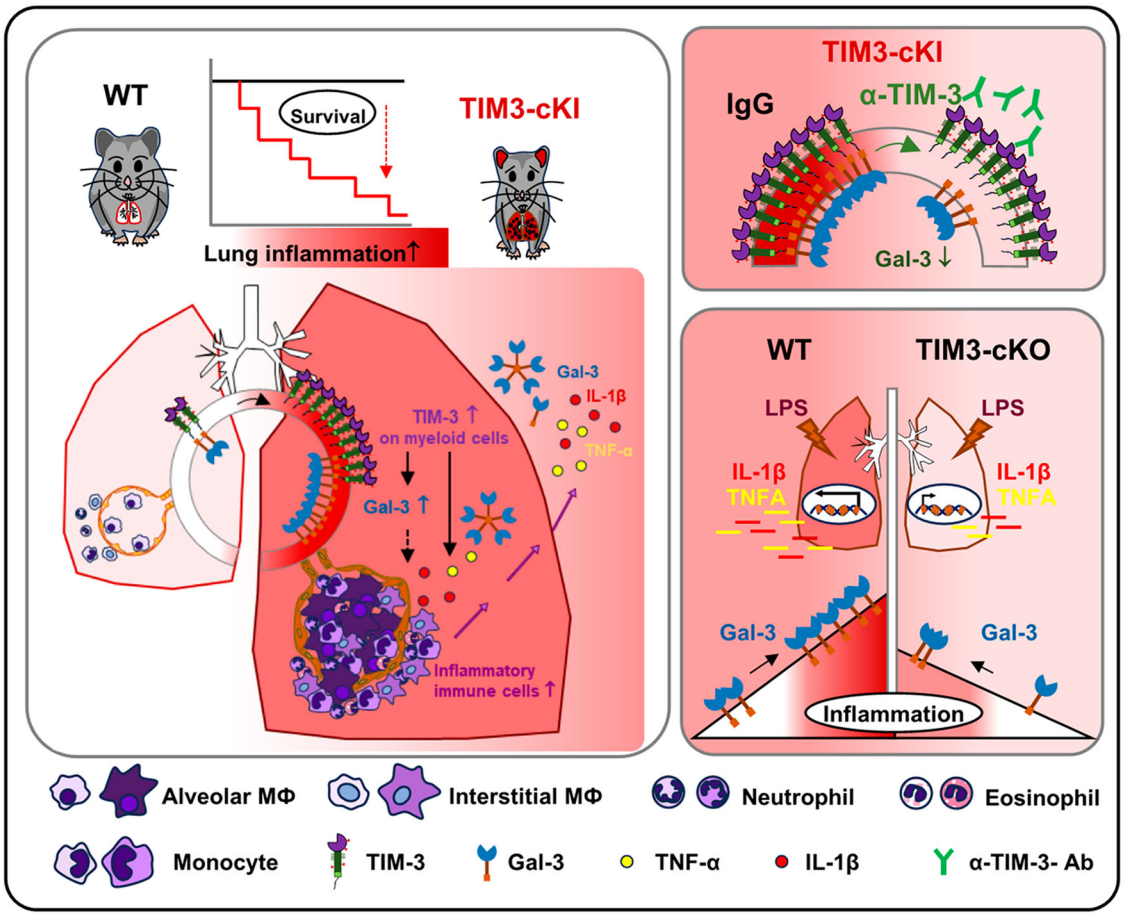

Fig. 10 | Schematic diagram depicting TIM-3-associated events in the lungs of conditional myeloid cell-specific TIM-3 knock-in and knock-out mice.

Collection and preparation of bronchoalveolar lavage fluid

Mice were tracheostomized and intubated and subjected thrice to bronchoalveolar lavage with 1 ml of PBS per lavage. The collected bronchoalveolar lavage fluid (BALF) samples were centrifuged at 400 g for 10 min at 4 °C. After centrifugation, the supernatant was concentrated using a protein concentrator (ThermoFisher Scientific, MA, USA) and used for measurement of secreted protein. Cell pellets from BALF were quantified using a hemocytometer and analyzed by flow cytometry after erythrocyte lysis (#WL2000; R&D System). For Giemsa staining (Modified Solution 32884; Sigma) and immunocytochemistry, BALF cells were first stabilized for 24 h in Dulbecco's modified Eagle's medium (DMEM) supplemented with 6 mg ml^{-1} glucose, 204 mg ml^{-1} L-glutamine, 100 U ml^{-1} penicillin/streptomycin (P/S), and 10% fetal bovine serum.

Preparation of bone-marrow-derived macrophages

Murine bone-marrow cells were isolated from femurs, and were plated in Dulbecco's modified Eagle's medium (DMEM) supplemented with M-CSF (20 ng/ml), 6 mg ml^{-1} glucose, 204 mg ml^{-1} L-glutamine, 100U ml^{-1} penicillin/streptomycin (P/S), and 10% fetal bovine serum. Then, cells were allowed to differentiate for 7 days into bone-marrow-derived macrophages.

Blocking of TIM-3 and inhibition of galectin-3

For TIM-3 blockade, 100 μg anti-TIM-3 (RMT3-23, BioXCell) per mouse or an equivalent doses of isotype control antibody (2A3, BioXCell) was administered by intraperitoneal (i.p.) injection in 100 μl PBS. Mice were injected every 3 days from 4 to 12 weeks of age. For galectin-3 inhibition, 1 mg/kg galectin-3 inhibitor GB1107 (1978336-61-6, MedChemExpress) per mouse or an equivalent dose of the vehicle was administered by intraperitoneal injection in 100 μl PBS every other day.

LPS-induced lung injury model

Mice were randomly divided into two groups: PBS, mock control; and LPS, lipopolysaccharide-treated (Sigma-Aldrich, L7770). Mice were intranasally challenged with a single dose of LPS in sterile PBS (10 μg in 30 μl) and examined at 24 h, 48 h, and 72 h post challenge. For histopathologic analysis of lung injury, lung sections were stained with H&E and scored quantitatively, as previously described in refs. 39,40. We also developed and applied a semiquantitative histopathologic scoring system based on bronchiolar inflammation and infiltrating cells, as shown in Supplementary Fig. 10. Blinded investigators scanned complete lung sections and scored lung inflammation from 0 to 3 using Phenochart 1.0.

Analysis of immune cell composition in bone marrow, spleen, and peripheral blood

At the time of sacrifice, bloods were harvested from the left ventricle using an EDTA-coated syringe, and were subsequently analyzed using an Auto Hematology Analyzer (BC-5000 Vet, Mindray). Mouse femur-derived bone marrow cells were obtained by repeated flushing of the bone shaft with PBS using a syringe. The harvested sample was then filtered through a 40-μm strainer and analyzed after erythrocyte lysis. To prepare splenocytes, the spleen was gently minced, filtered through a 40-μm strainer, and underwent erythrocyte lysis before analysis. The absolute cell numbers in bone marrow and spleen were calculated based on the total cell count and the frequence of cell subsets determined by flow cytometry.

Immunostaining

For immunohistochemistry, paraffin-embedded lung sections were deparaffinized in xylene and rehydrated via a graded ethanol series, and subjected to antigen retrieval (#00-4956, Invitrogen). For immunocytochemistry, cells were stabilized on coverslips and fixed in ice-cold 4% PFA at 4 °C for 30 min. The sections and cells were blocked for 1 h with 5% normal serum from the same host species used to generate the labeled secondary antibody. The sections and cells were then incubated at 4 °C overnight with the following primary antibodies, rabbit anti-TIM-3 (1:100; #ab185703, Abcam), goat anti-Galectin-3 (1:100; #AF1197, R&D Systems), and rat anti-F4/80 (1:100; #ab6640, Abcam). The sections and cells were washed and incubated with Alexa Fluor 488-labeled donkey anti-rabbit (1:400; #A-21206, Invitrogen), Alexa Fluor 546-labeled donkey anti-goat (1:400; #A-11056, Invitrogen), and Alexa Fluor 647-labeled donkey anti-rat secondary antibodies (1:400; #ab150155, Abcam) at room temperature for 1 h. The sections and cells were washed, subjected to nuclear staining with Hoechst 33342, and mounted with fluorescent mounting medium (Dako). Images were obtained using an LSM780 confocal microscope and analyzed by the Zen software (Carl Zeiss).

Flow cytometry

Flow cytometry was performed using FACSVerse system (BD Biosciences) and the following antibodies: mouse fluorescein-isothiocyanate (FITC)-anti-Ly-6G (1A8-Ly6g; eBioscience), phycoerythrin (PE)-anti-Siglec-F (1RNM44N; eBioscience), peridinin-chlorophyll-protein complex (PerCP)/Cy5.5-anti-F4/80 (BM8; eBioscience), PE/Cy7-anti-CD11b (M1/70; eBioscience), allophycocyanin (APC)-anti-Ly-6C (HK1.4; Biolegend), APC-eFluor780-anti-CD11c (N418; eBioscience), Brilliant-Violet-421 (BV421)-anti-TIM-3 (RMT3-23; Biolegend), Brilliant-Violet-510 (BV510)-anti-CD45 (30-F11; Biolegend), FITC-anti-Gr-1 (RB6-8C5; eBioscience), PE-anti-Galectin-3 (eBioM3/38; eBioscience), PE-anti-CD4 (GK1.5; eBioscience), APC-anti-CD8 (53-6.7; eBioscience), and APC-anti-Siglec-F (S17007L; Biolegend) for 30 min at 4 °C. Data were analyzed with FlowJo software (TreeStar).

Bulk RNA-sequencing

Total RNA (100 ng) was applied to construct a sequencing library using a SureSelect RNA Direct kit (Agilent) according to the manufacturer's protocol. Briefly, the total RNA was converted to cDNA and amplified with PCR to generate a cDNA library. For capture of mouse exonic regions, we used an Agilent SureSelect XT Mouse All Exon kit according to the standard Agilent SureSelect Target Enrichment protocol. The final purified product was quantified using a KAPA Library Quantification kit for Illumina Sequencing platforms (KAPA BIOSYSTEMS, #KK4854) according to the qPCR Quantification Protocol Guide. The product was qualified using TapeStation D1000 ScreenTape (Agilent Technologies, #5067-5582). The indexed libraries were loaded to an Illumina NovaSeq (Illumina, Inc., San Diego, CA, USA), and paired-end (2 × 100 bp) sequencing was performed by the Macrogen Incorporated.

RT-PCR and quantitative real-time RT-PCR

Total RNA was isolated using Easy-Blue (iNtRON, Korea), and cDNA was synthesized using avian myeloblastosis virus reverse transcriptase (TaKaRa, Japan) according to the manufacturer's instructions. Quantitative real-time PCR was performed with a Roche LightCycler 480 Real-Time PCR System (Roche Applied Science) using a QuantiFast SYBR Green PCR kit (Qiagen). LigthCycler 480 Quantification Software Version 1.5 was used for real-time PCR analysis. The utilized primers were listed in Supplementary Table 1.

Western blot analysis

Samples for western blot analysis were prepared as previously described previously[7]. The samples were separated by SDS–polyacrylamide gel electrophoresis, transferred to nitrocellulose membranes, and incubated at 4 °C with the following primary antibodies: goat anti-Galectin-1 (1:1,000; #AF1245, R&D Systems), rabbit anti-Galectin-3 (1:1,000; #12733, Cell Signaling Technologies), rat anti-Galectin-9 (1:500; #137901, Biolegend), mouse anti-β-Actin (1:2,000; #3700, Cell Signaling Technologies). The membranes were then incubated with the following secondary antibodies peroxidase-conjugated rabbit anti-goat (1:5000; #SA007-500, GenDEPOT), peroxidase-conjugated goat anti-rabbit (1:5000; #BR1706515, Bio-Rad), and peroxidase conjugated goat anti-mouse (1:5000; #BR1706516, Bio-Rad). The results were visualized using an enhanced chemiluminescence system, and quantified by densitometric analysis (Image J software, NIH). All experiments were performed independently at least three times.

ELISA

Mouse ELISA kits were used to measure the concentrations of TNF-α (#SMTA00B, R&D systems), IL-1β (#ab197742, Abcam), and galectin-3 (#DY1197, R&D systems) in BALF from FSF-TIM3, FSF-TIM3/*LysM*-Cre$^{+/-}$, and FSF-TIM3/*LysM*-Cre$^{+/+}$ mice. The plates were read at 450 nm on a microplate reader (Molecular Device).

Statistics and Reproducibility

All data are presented as the mean ± SD (n = number of individual samples). All statistical analyses were performed using GraphPad Prism 8 (GraphPad Software). Data shown are representative of three independent experiments. One-way ANOVA with Tukey's test and Two-way ANOVA with Sidak's test were used for multiple comparisons. A two-tailed Student's t test was used for when two conditions were compared. $P < 0.05$ was considered significant difference. $^{*}P < 0.05$, $^{**}P < 0.01$, $^{***}P < 0.001$, $^{****}P < 0.0001$.

Reporting summary

Further information on research design is available in the Nature Portfolio Reporting Summary linked to this article.

Data availability

All data supporting the findings within this study are available in Supplementary Information. All source data for graphs in this study are provided in Supplementary Data file. Sequences of the oligonucleotide primers used in this study are provided in Supplementary Table 1. The bulk RNA-sequencing data from this study have been deposited in the GEO database under accession code GSE268660. All original data in this study are also available from the corresponding author upon reasonable request.

Received: 10 November 2023; Accepted: 22 August 2024;
Published online: 05 September 2024

References

1. Monney, L. et al. Th1-specific cell surface protein Tim-3 regulates macrophage activation and severity of an autoimmune disease. *Nature* **415**, 536–541 (2002).
2. Anderson, A. C. et al. Promotion of tissue inflammation by the immune receptor Tim-3 expressed on innate immune cells. *Science* **318**, 1141–1143 (2007).
3. Chiba, S. et al. Tumor-infiltrating DCs suppress nucleic acid-mediated innate immune responses through interactions between the receptor TIM-3 and the alarmin HMGB1. *Nat. Immunol.* **13**, 832–842 (2012).

4. Gleason, M. K. et al. Tim-3 is an inducible human natural killer cell receptor that enhances interferon gamma production in response to galectin-9. *Blood* **119**, 3064–3072 (2012).
5. Nebbia, G. et al. Upregulation of the Tim-3/galectin-9 pathway of T cell exhaustion in chronic hepatitis B virus infection. *PLoS One* **7**, e47648 (2012).
6. Koh, H. S. et al. The HIF-1/glial TIM-3 axis controls inflammation-associated brain damage under hypoxia. *Nat. Commun.* **6**, 6340 (2015).
7. Kim, H. S. et al. Glial TIM-3 Modulates Immune Responses in the Brain Tumor Microenvironment. *Cancer Res*. **80**, 1833–1845 (2020).
8. Romero, D. Immunotherapy: PD-1 says goodbye, TIM-3 says hello. *Nat. Rev. Clin. Oncol.* **13**, 202–203 (2016).
9. Schnell, A., Bod, L., Madi, A. & Kuchroo, V. K. The yin and yang of co-inhibitory receptors: toward anti-tumor immunity without autoimmunity. *Cell Res* **30**, 285–299 (2020).
10. Wolf, Y., Anderson, A. C. & Kuchroo, V. K. TIM3 comes of age as an inhibitory receptor. *Nat. Rev. Immunol.* **20**, 173–185 (2020).
11. Banerjee, H. & Kane, L. P. Immune regulation by Tim-3. *F1000Res.* **7**, 316 (2018).
12. Wynn, T. A. & Vannella, K. M. Macrophages in Tissue Repair, Regeneration, and Fibrosis. *Immunity* **44**, 450–462 (2016).
13. Puttur, F., Gregory, L. G. & Lloyd, C. M. Airway macrophages as the guardians of tissue repair in the lung. *Immunol. Cell Biol.* **97**, 246–257 (2019).
14. Robb, C. T., Regan, K. H., Dorward, D. A. & Rossi, A. G. Key mechanisms governing resolution of lung inflammation. *Semin Immunopathol.* **38**, 425–448 (2016).
15. Moldoveanu, B. et al. Inflammatory mechanisms in the lung. *J. Inflamm. Res.* **2**, 1–11 (2009).
16. Ardain, A., Marakalala, M. J. & Leslie, A. Tissue-resident innate immunity in the lung. *Immunology* **159**, 245–256 (2020).
17. Di Simone, S. K., Rudloff, I., Nold-Petry, C. A., Forster, S. C. & Nold, M. F. Understanding respiratory microbiome-immune system interactions in health and disease. *Sci. Transl. Med* **15**, eabq5126 (2023).
18. Thiemann, S. & Baum, L. G. Galectins and Immune Responses-Just How Do They Do Those Things They Do? *Annu Rev. Immunol.* **34**, 243–264 (2016).
19. Zhou, Y. et al. Galectin-3 Interacts with the CHI3L1 Axis and Contributes to Hermansky-Pudlak Syndrome Lung Disease. *J. Immunol.* **200**, 2140–2153 (2018).
20. Pugliese, G., Iacobini, C., Pesce, C. M. & Menini, S. Galectin-3: an emerging all-out player in metabolic disorders and their complications. *Glycobiology* **25**, 136–150 (2015).
21. Rabinovich, G. A. & Toscano, M. A. Turning 'sweet' on immunity: galectin-glycan interactions in immune tolerance and inflammation. *Nat. Rev. Immunol.* **9**, 338–352 (2009).
22. de Boer, R. A., Daniels, L. B., Maisel, A. S. & Januzzi, J. L. Jr State of the Art: Newer biomarkers in heart failure. *Eur. J. Heart Fail* **17**, 559–569 (2015).
23. Jiang, H. R. et al. Galectin-3 deficiency reduces the severity of experimental autoimmune encephalomyelitis. *J. Immunol.* **182**, 1167–1173 (2009).
24. James, R. E. et al. Loss of galectin-3 decreases the number of immune cells in the subventricular zone and restores proliferation in a viral model of multiple sclerosis. *Glia* **64**, 105–121 (2016).
25. Pilette, C. et al. Increased galectin-3 expression and intra-epithelial neutrophils in small airways in severe COPD. *Eur. Respir. J.* **29**, 914–922 (2007).
26. Bouffette, S., Botez, I. & De Ceuninck, F. Targeting galectin-3 in inflammatory and fibrotic diseases. *Trends Pharm. Sci.* **44**, 519–531 (2023).
27. Gao, P., Simpson, J. L., Zhang, J. & Gibson, P. G. Galectin-3: its role in asthma and potential as an anti-inflammatory target. *Respir. Res* **14**, 136 (2013).
28. Amani, M. F., Rolig, A. S. & Redmond, W. L. Intracellular Galectin-3 Is Essential for OX40-Mediated Memory CD8(+) T Cell Development. *J. Immunol.* **205**, 1857–1866 (2020).
29. Liu, Y. et al. Galectin-3 regulates microglial activation and promotes inflammation through TLR4/MyD88/NF-kB in experimental autoimmune uveitis. *Clin. Immunol.* **236**, 108939 (2022).
30. Boza-Serrano, A. et al. Galectin-3, a novel endogenous TREM2 ligand, detrimentally regulates inflammatory response in Alzheimer's disease. *Acta Neuropathol.* **138**, 251–273 (2019).
31. Priglinger, C. S. et al. Galectin-3 induces clustering of CD147 and integrin-beta1 transmembrane glycoprotein receptors on the RPE cell surface. *PLoS One* **8**, e70011 (2013).
32. MacKinnon, A. C. et al. Regulation of alternative macrophage activation by galectin-3. *J. Immunol.* **180**, 2650–2658 (2008).
33. Jia, W. et al. Indispensable role of Galectin-3 in promoting quiescence of hematopoietic stem cells. *Nat. Commun.* **12**, 2118 (2021).
34. Banerjee, H. et al. Expression of Tim-3 drives phenotypic and functional changes in Treg cells in secondary lymphoid organs and the tumor microenvironment. *Cell Rep.* **36**, 109699 (2021).
35. Avery, L., Filderman, J., Szymczak-Workman, A. L. & Kane, L. P. Tim-3 co-stimulation promotes short-lived effector T cells, restricts memory precursors, and is dispensable for T cell exhaustion. *Proc. Natl. Acad. Sci. USA* **115**, 2455–2460 (2018).
36. Duan, M. et al. CD11b immunophenotyping identifies inflammatory profiles in the mouse and human lungs. *Mucosal Immunol.* **9**, 550–563 (2016).
37. Nishi, Y. et al. Role of galectin-3 in human pulmonary fibrosis. *Allergol. Int* **56**, 57–65 (2007).
38. Kim, S. J. et al. Crosstalk between WNT and STAT3 is mediated by galectin-3 in tumor progression. *Gastric Cancer* **24**, 1050–1062 (2021).
39. Zeldin, D. C. et al. Airway inflammation and responsiveness in prostaglandin H synthase-deficient mice exposed to bacterial lipopolysaccharide. *Am. J. Respir. Cell Mol. Biol.* **25**, 457–465 (2001).
40. Klopfleisch, R. Multiparametric and semiquantitative scoring systems for the evaluation of mouse model histopathology–a systematic review. *BMC Vet. Res*. **9**, 123 (2013).
41. Faniyi, A. A., Hughes, M. J., Scott, A., Belchamber, K. B. R. & Sapey, E. Inflammation, ageing and diseases of the lung: Potential therapeutic strategies from shared biological pathways. *Br. J. Pharm.* **179**, 1790–1807 (2022).
42. Wang, Y. et al. Overexpression of TIM-3 in Macrophages Aggravates Pathogenesis of Pulmonary Fibrosis in Mice. *Am. J. Respir. Cell Mol. Biol.* **61**, 727–736 (2019).
43. Qiu, Y. et al. Tim-3-expressing CD4+ and CD8+ T cells in human tuberculosis (TB) exhibit polarized effector memory phenotypes and stronger anti-TB effector functions. *PLoS Pathog.* **8**, e1002984 (2012).
44. Wang, P. H. et al. The Trend of TIM3 Expression on T Cells in Patients With Nontuberculous Mycobacterial Lung Disease: From Immune Cell Dysfunction to Clinical Severity. *Front Immunol.* **12**, 738056 (2021).
45. Almkvist, J. & Karlsson, A. Galectins as inflammatory mediators. *Glycoconj. J.* **19**, 575–581 (2002).
46. Liu, F. T. & Stowell, S. R. The role of galectins in immunity and infection. *Nat. Rev. Immunol.* **23**, 479–494 (2023).
47. Humphries, D. C. et al. Galectin-3 inhibitor GB0139 protects against acute lung injury by inhibiting neutrophil recruitment and activation. *Front Pharm.* **13**, 949264 (2022).
48. Erriah, M. et al. Galectin-3 enhances monocyte-derived macrophage efferocytosis of apoptotic granulocytes in asthma. *Respir. Res* **20**, 1 (2019).

49. Snarr, B. D. et al. Galectin-3 enhances neutrophil motility and extravasation into the airways during Aspergillus fumigatus infection. *PLoS Pathog.* **16**, e1008741 (2020).
50. Chen, Y. J. et al. Galectin-3 Enhances Avian H5N1 Influenza A Virus-Induced Pulmonary Inflammation by Promoting NLRP3 Inflammasome Activation. *Am. J. Pathol.* **188**, 1031–1042 (2018).
51. Hirani, N. et al. Target inhibition of galectin-3 by inhaled TD139 in patients with idiopathic pulmonary fibrosis. *Eur. Respir. J.* **57**, 200559 (2021).
52. Liao, M. et al. Single-cell landscape of bronchoalveolar immune cells in patients with COVID-19. *Nat. Med*. **26**, 842–844 (2020).
53. Garcia-Revilla, J., Deierborg, T., Venero, J. L. & Boza-Serrano, A. Hyperinflammation and Fibrosis in Severe COVID-19 Patients: Galectin-3, a Target Molecule to Consider. *Front. Immunol.* **11**, 2069 (2020).
54. Cervantes-Alvarez, E. et al. Galectin-3 as a potential prognostic biomarker of severe COVID-19 in SARS-CoV-2 infected patients. *Sci. Rep.* **12**, 1856 (2022).
55. Nangia-Makker, P., Balan, V. & Raz, A. Regulation of tumor progression by extracellular galectin-3. *Cancer Microenviron.* **1**, 43–51 (2008).
56. Hara, A. et al. Galectin-3 as a Next-Generation Biomarker for Detecting Early Stage of Various Diseases. *Biomolecules* **10**, 389 (2020).
57. Jeon, S. B. et al. Galectin-3 exerts cytokine-like regulatory actions through the JAK-STAT pathway. *J. Immunol.* **185**, 7037–7046 (2010).
58. Ikemori, R. Y. et al. Galectin-3 up-regulation in hypoxic and nutrient deprived microenvironments promotes cell survival. *PLoS One* **9**, e111592 (2014).
59. Li, J., Shen, H., Owens, G. K. & Guo, L. W. SREBP1 regulates Lgals3 activation in response to cholesterol loading. *Mol. Ther. Nucleic Acids* **28**, 892–909 (2022).
60. Wang, L. & Guo, X. L. Molecular regulation of galectin-3 expression and therapeutic implication in cancer progression. *Biomed. Pharmacother.* **78**, 165–171 (2016).
61. Lee, J. et al. Phosphotyrosine-dependent coupling of Tim-3 to T-cell receptor signaling pathways. *Mol. Cell Biol.* **31**, 3963–3974 (2011).
62. de Mingo Pulido, A. et al. The inhibitory receptor TIM-3 limits activation of the cGAS-STING pathway in intra-tumoral dendritic cells by suppressing extracellular DNA uptake. *Immunity* **54**, 1154–1167.e1157 (2021).
63. de Mingo Pulido, A. et al. TIM-3 Regulates CD103(+) Dendritic Cell Function and Response to Chemotherapy in Breast Cancer. *Cancer Cell* **33**, 60–74.e66 (2018).
64. Dixon, K. O. et al. TIM-3 restrains anti-tumour immunity by regulating inflammasome activation. *Nature* **595**, 101–106 (2021).
65. Ausejo-Mauleon, I. et al. TIM-3 blockade in diffuse intrinsic pontine glioma models promotes tumor regression and antitumor immune memory. *Cancer Cell* **41**, 1911–1926.e1918 (2023).
66. Kearley, J., McMillan, S. J. & Lloyd, C. M. Th2-driven, allergen-induced airway inflammation is reduced after treatment with anti-Tim-3 antibody in vivo. *J. Exp. Med.* **204**, 1289–1294 (2007).
67. Gayden, T. et al. Germline HAVCR2 mutations altering TIM-3 characterize subcutaneous panniculitis-like T cell lymphomas with hemophagocytic lymphohistiocytic syndrome. *Nat. Genet* **50**, 1650–1657 (2018).
68. Jayaraman, P. et al. Tim3 binding to galectin-9 stimulates antimicrobial immunity. *J. Exp. Med*. **207**, 2343–2354 (2010).
69. Sabatos, C. A. et al. Interaction of Tim-3 and Tim-3 ligand regulates T helper type 1 responses and induction of peripheral tolerance. *Nat. Immunol.* **4**, 1102–1110 (2003).
70. Isshiki, T. et al. Cutting Edge: Anti-TIM-3 Treatment Exacerbates Pulmonary Inflammation and Fibrosis in Mice. *J. Immunol.* **199**, 3733–3737 (2017).

Acknowledgements

We thank S. Kang (Animal Molecular Imaging), M. Kim (Microscopy Core), T. Kim (Flow cytometry Core), and members of Laboratory Animal Research Core for expert assistance and suggestions. We are especially grateful to Dr. Eun-Kyung Hong from the department of pathology for her help with the histopathological analysis of tissues. We also appreciate Drs. Eun Kyung Lee, Ki-Wook Kim, Joonha Kwon, and Chungyong Han for their helpful discussions. This work was supported by the National Cancer Center (NCC-2410910) and National Research Foundation of Korea (NRF-2021R1A2C2012528).

Author contributions

K.S.K. and E.J.P. conceived and designed research studies. K.S.K., C.L., H.K., S.J.G., H.J.Y., and S.B.W., performed experiments and analyzed data. H.L., S.S.K., Y.S.L., and L.P.K. contributed to the design experiments and discussed the data. K.S.K. and E.J.P. wrote the manuscript. E.J.P. supervised the study.

Competing interests

The authors declare no competing interests.

Additional information

Supplementary information The online version contains supplementary material available at https://doi.org/10.1038/s42003-024-06762-w.

Correspondence and requests for materials should be addressed to Eun Jung Park.

Peer review information *Communications Biology* thanks Manu Rangachari, Yochai Wolf and the other, anonymous, reviewer(s) for their contribution to the peer review of this work. Primary Handling Editors: Si Ming Man and Dario Ummarino.